

# **REPORT RDU1703145**

## **OPTIMIZATION OF SOLENOID DRIVER AND CONTROLLER FOR GASEOUS FUEL HIGH-PRESSURE DIRECT INJECTOR USING MODEL- BASED APPROACH**

**FACULTY OF MECHANICAL ENGINEERING**

**PROJECT LEADER:  
MR. MOHD FADZIL BIN ABDUL RAHIM**

**UNIVERSITI MALAYSIA PAHANG**

**UMP**

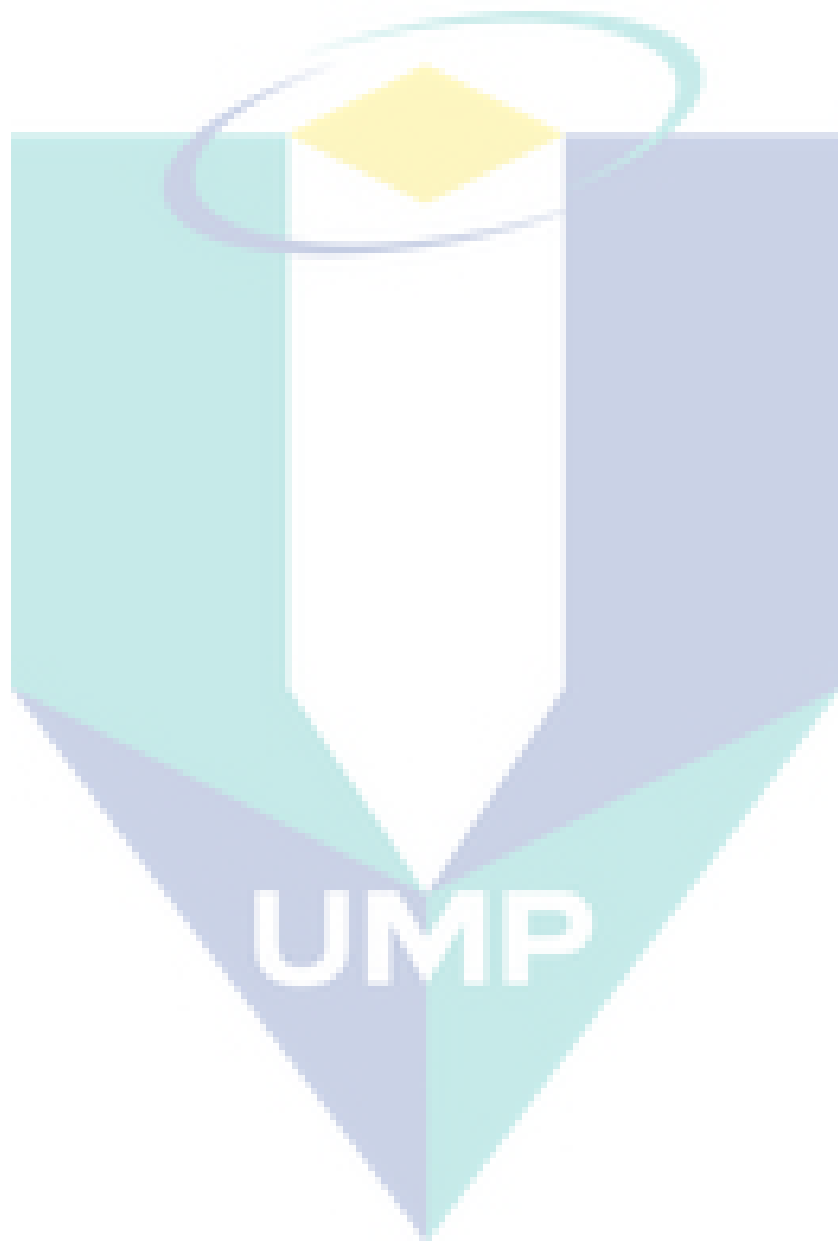


## TABLE OF CONTENT

<b>TABLE OF CONTENT</b>	<b>i</b>
<b>LIST OF TABLES</b>	<b>v</b>
<b>LIST OF FIGURE</b>	<b>vi</b>
<b>LIST OF ABBREVIATIONS</b>	<b>viii</b>
<b>LIST OF SYMBOLS</b>	<b>ix</b>
<b>ABSTRACT</b>	<b>x</b>
<b>1 INTRODUCTION</b>	<b>11</b>
1.1 Background of study	11
1.2 Problem statement	11
1.3 Research questions	12
1.4 Objective of study	12
1.5 Scope of study	13
1.6 Hypothesis	13
1.7 Project timeline	14
<b>2 LITERATURE REVIEW</b>	<b>16</b>
2.1 Introduction	16
2.2 CNG as Fuel	16
2.3 Type of injection system	18
2.3.1 Single-point or throttle-body injection	18

2.3.2	Port or multipoint fuel injection	19
2.3.3	Sequential fuel injection	20
2.3.4	Direct injection	20
2.4	Injector for CNG	22
2.5	Mass flow rate	23
2.6	Driver and controller	23
2.6.1	Saturated driver (high impedance)	23
2.6.2	Peak and hold driver (low impedance/current regulated)	24
2.7	Injector testing	26
2.8	Optimization of injector	27
<b>3</b>	<b>METHODOLOGY</b>	<b>29</b>
3.1	Introduction	29
3.2	Flowchart	29
3.3	ANSYS Maxwell simulation	31
3.3.1	Power losses model	31
3.3.2	Electromagnetic and Mechanical losses model	32
3.3.3	The injector computational domain	33
3.3.4	Electromagnetic simulation procedure	35
3.3.5	Maxwell circuit editor procedure	37
3.4	Square wave experimental study	37
3.4.1	Injector Specification	38
3.4.2	Instrumentation setup and layout	40

3.4.3	Square wave driver and controller	43
3.5	Two Stage signal wave experimental study	44
3.6	Square wave simulation study	45
3.6.1	The electromagnetic model	45
3.6.2	The mechanical model	46
3.6.3	The flow model	48
3.6.4	The simulation setup	51
3.7	Two stage signal wave simulation study	53
<b>4</b>	<b>EXPECTED RESULT</b>	<b>58</b>
4.1	ANSYS Maxwell simulation result	58
4.1.1	Magnetic Field Intensity	58
4.1.2	Core Losses	59
4.2	Square wave experimental result	62
4.2.1	Case 1: effect of injection pressure	62
4.2.2	Case 2: effect of injection duration	63
4.2.3	Case 3: Effect of Injection Frequency	64
4.3	Two stage signal wave experimental result	65
4.3.1	Square wave and two stage signal wave profile	65
4.3.2	Case 1: fixed duration time	66
4.3.3	Case 2: increasing duration time	67
4.4	Square wave simulation result	69
4.4.1	Validation of Simulation Model (Injection Pressure)	69

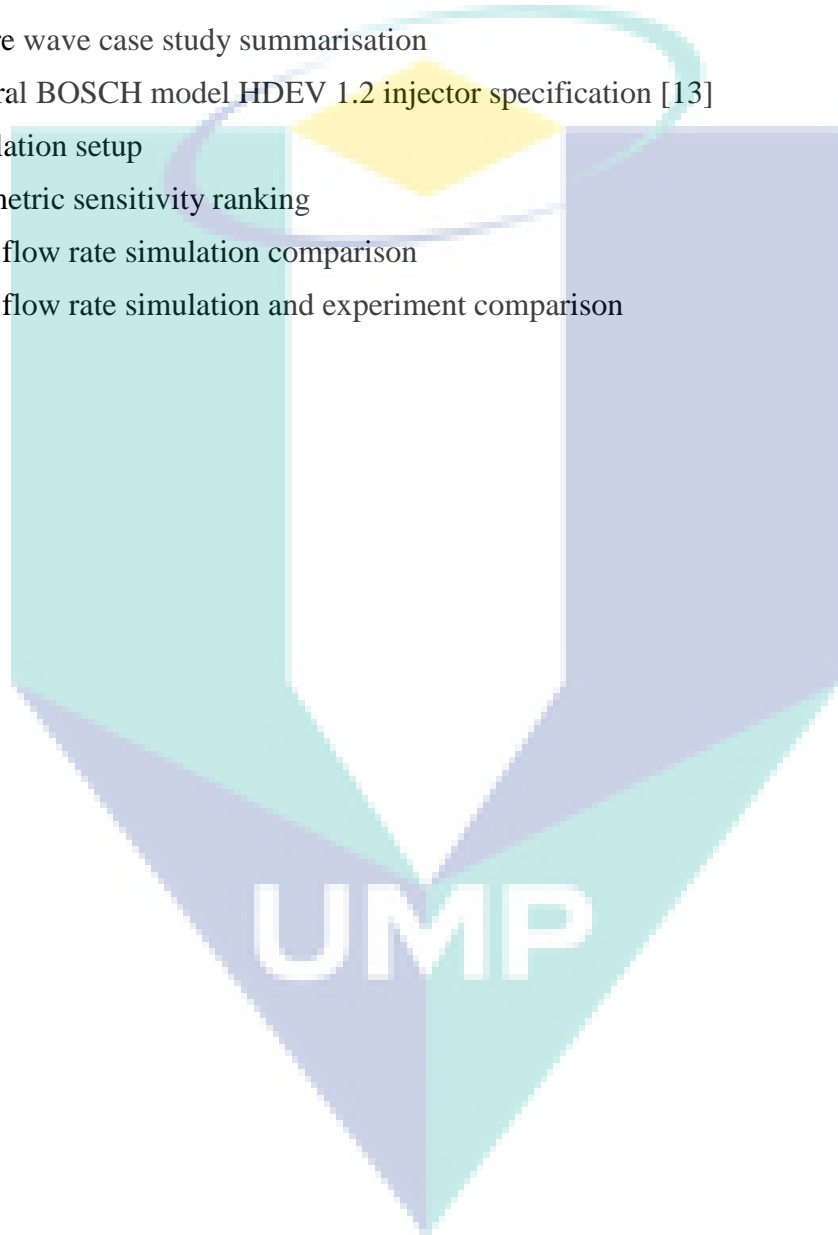
4.4.2	Validation of Simulation Model (Injection Duration)	70
4.4.3	Parametric Study of Input Voltage	71
4.4.4	Parametric Study of Spring Constant	72
4.4.5	Parametric Study of Nozzle Diameter	73
4.4.6	Parameter Study of Armature Mass	73
4.4.7	Parametric Sensitivity Ranking	74
4.5	Two stage signal wave simulation result	75
4.5.1	Nozzle area	75
4.5.2	Solenoid force	76
4.5.3	Total mass inject	77
4.5.4	Mass flow rate	78
4.5.5	Result comparison	78
<b>5</b>	<b>CONCLUSION</b>	<b>80</b>
	<b>REFERENCES</b>	<b>82</b>



UMP

## LIST OF TABLES

Table 1: Natural gas properties [9]	17
Table 2: Thermodynamics properties of CNG, gasoline and diesel [9]	18
Table 3 : Simulation Parameter	36
Table 4 : Square wave case study summarisation	38
Table 5 : General BOSCH model HDEV 1.2 injector specification [13]	38
Table 6 : Simulation setup	51
Table 7 : Parametric sensitivity ranking	74
Table 8 : Mass flow rate simulation comparison	78
Table 9 : Mass flow rate simulation and experiment comparison	79



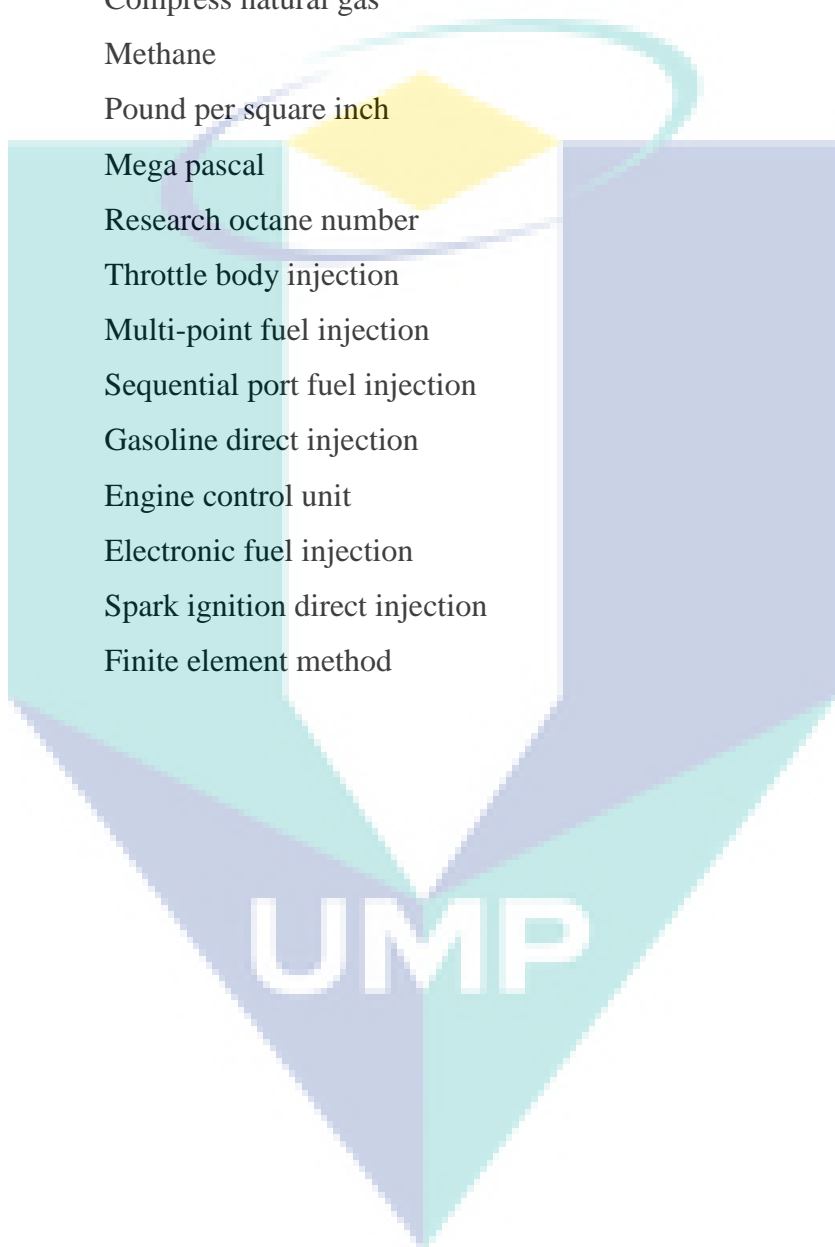
## LIST OF FIGURE

Figure 1: Single point/throttle body injection system	19
Figure 2: Multi point/port injection system	20
Figure 3: Direct injection system	21
Figure 4: Comparison between peak and hold driver with saturated driver	25
Figure 5 : 2D model of injector	34
Figure 6 : Simulation Flow Chart	35
Figure 7 : Simulation 2D meshing	36
Figure 8 : Injector circuit [5]	37
Figure 9 : BOSCH model HDEV 1.2 injector physical appearance	39
Figure 10 : Schematic diagram of the experimental setup	40
Figure 11 : The injector being clamped to the test rig	41
Figure 12: The custom test rig bolt on table	41
Figure 13: The fume extractor being used in the experiment	42
Figure 14: The CNG tank on top of the weighting scale	42
Figure 15: The connection of driver and controller circuit for the injector	43
Figure 16 : Schematic diagram for square wave driver and controller circuit	43
Figure 17 : Schematic diagram of two stage signal wave driver	44
Figure 18 : Pintle free body diagram [13]	47
Figure 19 : Definitions of effective flow area for nozzle flow calculation [15]	50
Figure 20 : MATLAB Simulink block diagrams of the injector simulation model	51
Figure 21 : Square wave signal	53
Figure 22 : Signal 1	54
Figure 23 : Signal 2	54
Figure 24 : Signal 3	55
Figure 25 : Signal 4	55
Figure 26 : Signal 5	56
Figure 27 : Signal 6	56
Figure 28 : MATLAB Simulink block diagrams of the modified injector simulation model	57



Figure 29 : Magnetic Field Intensity simulation	58
Figure 30 : Core losses at 6V	59
Figure 31 : Core losses at 9V	60
Figure 32 : Core losses at 12V	61
Figure 33 : Comparison of injection pressure with mass flow rate	62
Figure 34 : Comparison of mass flow rate on different injection duration	63
Figure 35 : The measured average mass flow rate at different injection frequency	64
Figure 36 : Square wave profile at 50bar	65
Figure 37 : Two stage signal wave profile at 50bar	65
Figure 38 : CNG tank weight vs injection duration for square wave	66
Figure 39 : CNG tank weight vs injection duration for two stage signal wave	67
Figure 40 : Mass flow rate of square wave and two stage signal wave	68
Figure 41 : Comparison between experiment and simulation injection pressure	69
Figure 42 : Comparison between experiment and simulation injection duration	70
Figure 43 : Simulation result of input voltage versus mass flow rate	71
Figure 44 : Simulation result of spring constant versus mass flow rate	72
Figure 45 : Simulation result of nozzle diameter versus mass flow rate	73
Figure 46 : Simulation result of armature mass versus mass flow rate	74
Figure 47 : Nozzle area simulation result	75
Figure 48 : Solenoid force simulation result	76
Figure 49 : Total mass inject simulation result	77
Figure 50 : Mass flow rate simulation result	78

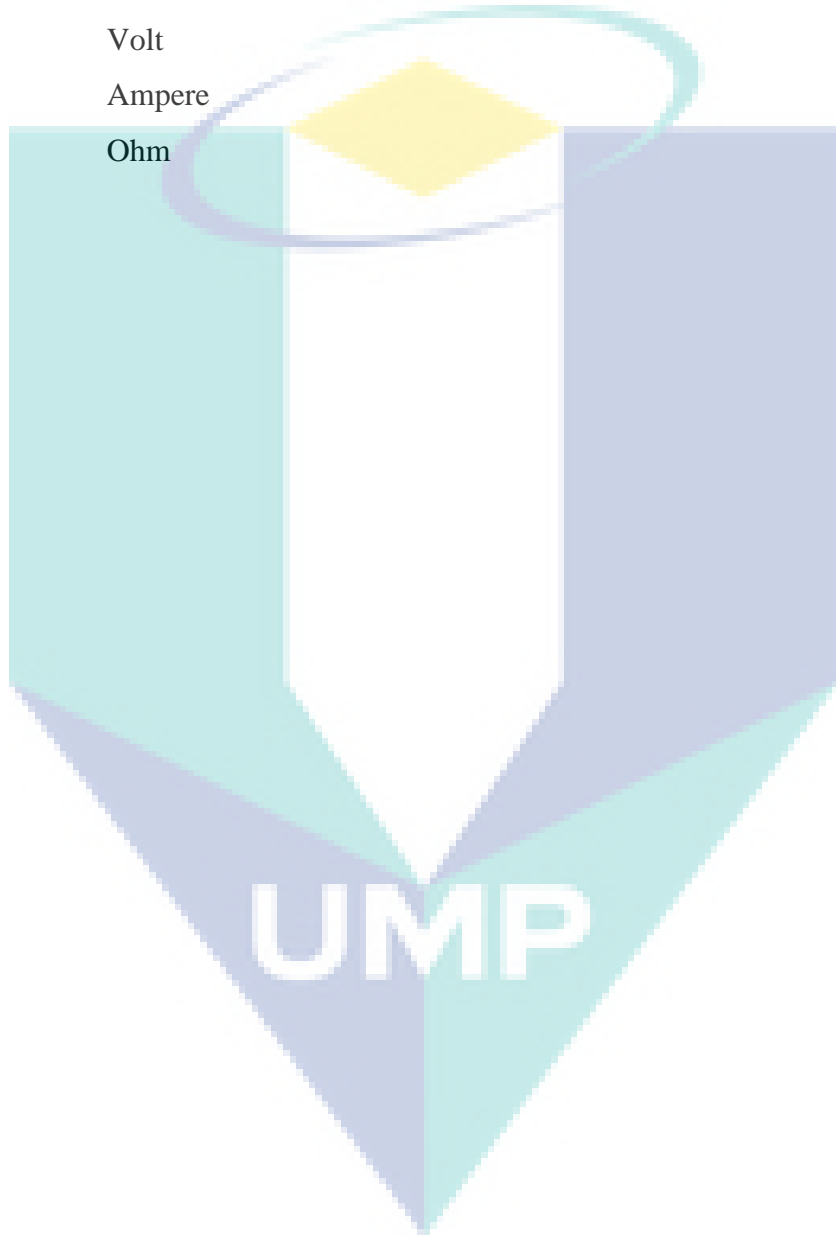
## LIST OF ABBREVIATIONS



CNG	Compress natural gas
CH <sub>4</sub>	Methane
PSI	Pound per square inch
MPa	Mega pascal
RON	Research octane number
TBI	Throttle body injection
MPFI	Multi-point fuel injection
SPFI	Sequential port fuel injection
GDI	Gasoline direct injection
ECU	Engine control unit
EFI	Electronic fuel injection
SIDI	Spark ignition direct injection
FEM	Finite element method

## LIST OF SYMBOLS

ms	Millisecond
V	Volt
A	Ampere
$\Omega$	Ohm



## ABSTRACT

Direct injection system for CNG fuel is a new development hence; the losses in solenoid drive direct fuel injector are not yet studied. The losses are suspected as the major cause for fluctuating injector mass flow rate which affected the engine torque stability due to the power losses. Solenoid drive internal losses are the major contribution to power losses. The key factor is non optimal driver current and voltage. Purpose of this study is to investigate the most influential type of power losses which affect the mass flow rate consistency and optimization of driver current and voltage to increase the controllability of the mass flow rate. Model-based optimization is the main method used to obtain the optimal setting for current and voltage of injector driver. In order to generate the experimental model by using offline system identification, cause-effect study is carried out by static and dynamic test. From the study, the primarily expected outcome are relationship between input and output variables of the injector flow, identification of significant losses based on the dynamic response analysis and optimum control of injector driver which will maximize the controllability of the injector flow rate. The results obtained from the study are important to increase the effectiveness of control strategies embedded in the development of dedicated driver and controller for the gaseous fuel direct injector.

The logo for UMP (Universitas Muhammadiyah Purwokerto) is a large, stylized shield shape. It is divided into four quadrants by a white cross. The top-left and bottom-right quadrants are light blue, while the top-right and bottom-left quadrants are light green. The letters 'UMP' are written in white, bold, sans-serif font across the center of the shield.

UMP



## INTRODUCTION

### 1.1 Background of study

Emissions produced by internal combustion engine running on conventional fossil fuels are of major concern nowadays and have become major research topic. Vehicle manufacturers are enforced with more strict emission regulation year by year. One of the most seeks and well established approach is by converting a conventional fossil fuels vehicle into cleaner alternatives. The most preferable alternative for gasoline and diesel accepted widely around the globe is compressed natural gas (CNG). Direct injection of CNG has been identified as the most capable technology to boost CNG engine performance [1]. However, the commercial CNG direct injector available in the market is expensive and not affordable until nowadays. Currently, the easiest step to develop dedicated gaseous fuel direct injector system is by converting the existing liquid fuel direct injector to run on gas. But the conversion of liquid fuel direct injector alters the losses and efficiency of the injector from manufacturer benchmarked. To suppress the losses of the injector driver, controller and control strategies of the electronic control unit of the injector, recalibrations are required for different fluid material [2]. The direct injection system for CNG fuel is newly developed. Thus, the losses in solenoid drive direct fuel injector are not yet studied as compared to gasoline and diesel. The losses are suspected as the major cause for fluctuating injector mass flow rate. The fluctuating mass flow rate affects the engine torque stability. The root of these losses is due to the power losses. Major contribution to power losses is the solenoid drive internal losses. The key factor is non optimal driver current and voltage.

### 1.2 Problem statement

Power losses in solenoid drive of direct fuel injector are contributed by Ohmic loss, core loss, eddy current loss, solid loss, and stranded loss. Major factor affecting the power losses is the control strategy of

the injector driver [3]. The main parameters of the driver's control strategy are the boost current and voltage. However, most of the reported study on the power losses are concentrated on the application of direct injector for gasoline fuel such as [4], [5] and diesel [6] which are supplied to the injector in liquid form. So far, no study has been conducted on direct fuel injector for gaseous fuel especially CNG. Therefore, a study is needed to clarify the most significant losses in the direct fuel injector for CNG application. The knowledge on significant losses shall be used to conduct optimization of driver and controller's parameters. Optimized driver and controller parameter will improve the controllability and stability of the injector mass flow rate. The study is important in the development of dedicated driver and controller for direct fuel injector of gaseous fuel especially CNG [7]. The driver and controller are the key component of CNG retrofitted direct fuel injection system. The availability of retrofitted direct fuel injected system to the end user will enhance effective and optimum usage of energy sources in the country [8]. The use of CNG in addition, will promote fossil fuel diversification and provide energy security in the future.

### 1.3 Research questions

1. How to account and measure the different type of losses in an electromagnetic drive injector?
2. Can the losses be reduced if suitable voltage and current profile able to be supplied by the injector driver and controller?
3. What is the strategy to minimize the losses and maximize the performance of an injector to supply sufficient fuel to the engine at each engine operating mode?

### 1.4 Objective of study

The objectives of this research are as follows:

1. To investigate and clarify the most influential losses which affect an electromagnetic drive direct-injector flow rate.
2. To minimise the losses and improve consistency of the injector mass flow rate via modelling-based optimization approach.

## 1.5 Scope of study

- 1) Development of testing procedure of dynamic analysis of the injector during no fuel and with fuel condition.
- 2) Investigation of relationship between injector input-output parameters and to identify the influential losses terms in injector operation.
- 3) System identification of the injector to produce dynamic injector model.
- 4) Proposing optimized driver and controller parameter setup for the identified dynamic model.

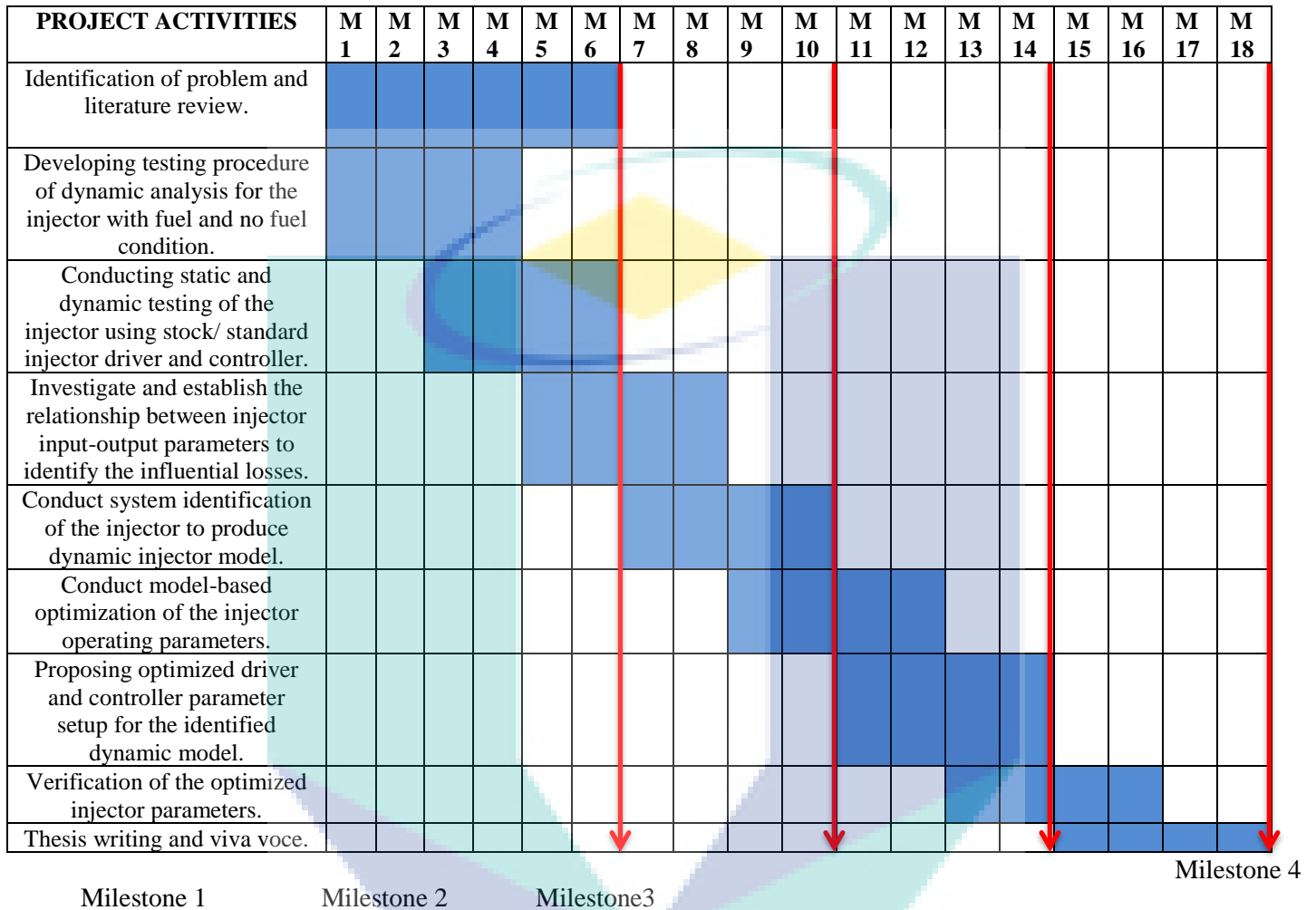
## 1.6 Hypothesis

The power losses in the solenoid drive coil are the main cause for the inconsistencies of injector's mass flow rate. IF the losses are adequately minimised through optimisation of the driver current and voltage, THEN controllability and stability of the injector mass flow rate can be improved and randomly fluctuated flow rates can be reduced.

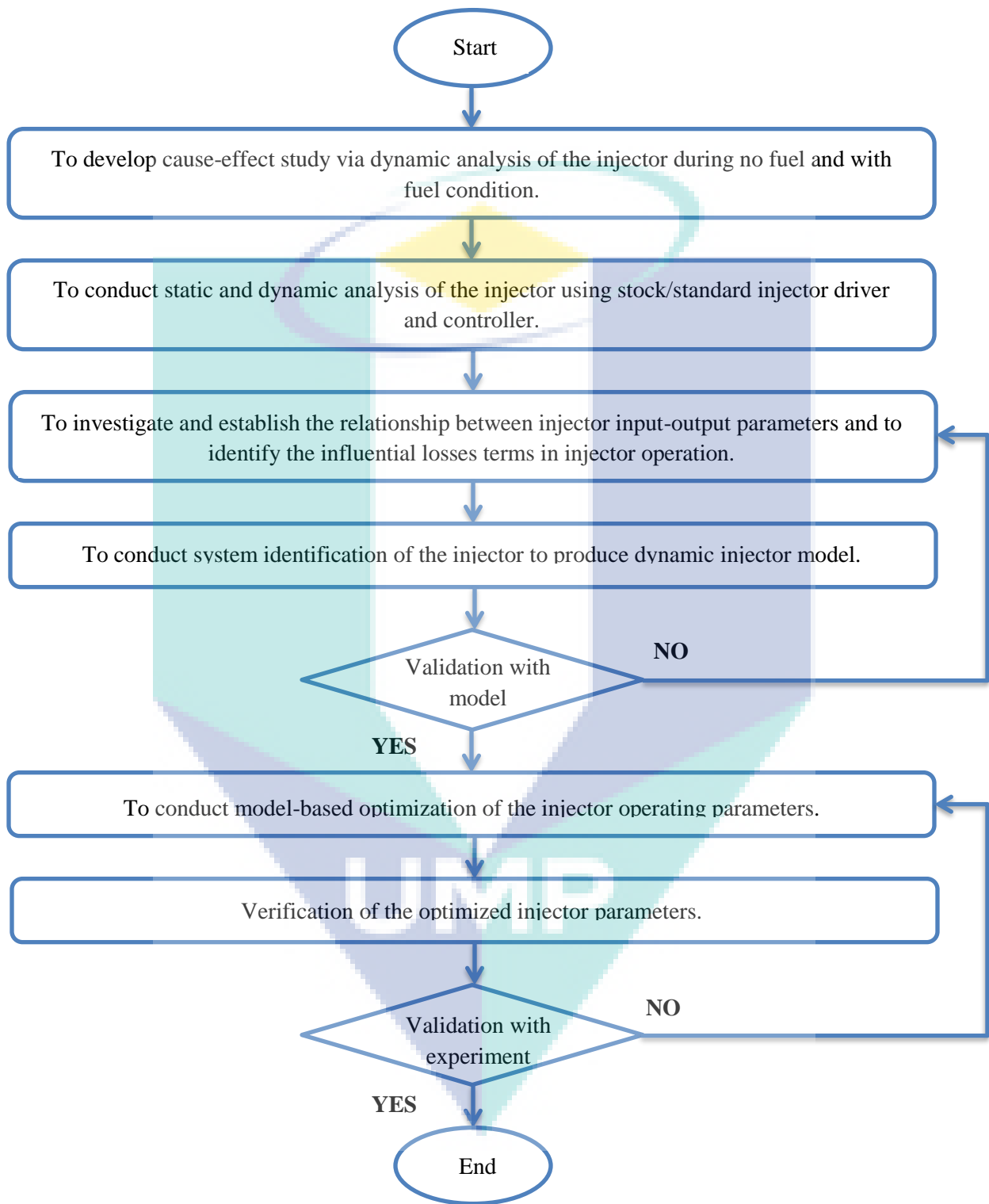
The logo for UMP (Universiti Malaysia Perlis) is a large, stylized shield shape. It is divided into four quadrants by a white 'V' shape pointing downwards. The top-left and bottom-right quadrants are light blue, while the top-right and bottom-left quadrants are light green. The letters 'UMP' are written in white, bold, sans-serif font across the center of the shield.

UMP

## 1.7 Project timeline







## LITERATURE REVIEW

### 2.1 Introduction

The primary objective of this chapter is to discuss the fundamental aspects of injection system and injector characteristic. Next, followed by suggestion of methods to identify the affected losses and the efficiency of the injector hence propose a suitable experimental and analysis of data. Thus, leading to understanding the application of the methodology for this project.

### 2.2 CNG as Fuel

Compressed natural gas (CNG) is a fuel which can replace Petrol, Diesel and LPG in their respective application. The combustion of CNG produces lesser and fewer undesirable gases than another fuels mentioned. CNG is a colourless, tasteless, odourless, and non-toxic gas made by compressing natural gas mainly composed of methane ( $\text{CH}_4$ ). Less than 1 percent of the volume it occupies at standard atmospheric pressure. It is stored and distributed in hard cylindrical or spherical containers at a pressure of 20-25 MPa equivalents to 200-250 bar, or 3,000-3,600 PSI.[9] CNG may be collected from gas wells or found in conjunction with crude oil production. CNG is lighter than air and thus will quickly disperse in the case of leak, giving it a significant safety advantage over others fuel.

**Table 1: Natural gas properties [9]**

Constituent	Volume (%)
Methane	95.3
Ethane	2.16
Propane	0.19
N-Butane	0.02
Iso-Butane	0.02
N-Pentane	0.00
Iso-Pentane	0.01
Hexanes Plus	0.00
Nitrogen	1.86
Carbon Dioxide	0.44
Oxygen	0.00
Hydrogen	0.00

Their significant advantages over other fuels are they were proven to be holding substantial reserves with a cleaner combustion and competitive market price [10]. CNG also has a higher RON number compared to gasoline and diesel hence promoting better knock resistance [11] and higher hydrogen to carbon ratio [12] therefore making it suitable as transportation fuel. CNG is used in traditional internal combustion engine that have been modified or in vehicles which were manufactured for CNG use, either dedicated, dual fuel or bi-fuel. CNG flows through a fuel line from the compression tanks into a regulator and gets injected into the engine just like gasoline. CNG will only ignite within an acceptable range of saturation. If too much natural gas, there will be not enough oxygen to ignite and vice versa. This delicate balance makes CNG vehicles inherently safer than traditional fuel vehicles. In response to high fuel prices and environmental concerns, CNG vehicles that were being use around the world are steadily increasing and also starting to be used in public transportation.

**Table 2: Thermodynamics properties of CNG, gasoline and diesel [9]**

<b>Properties</b>	<b>CNG</b>	<b>Gasoline</b>	<b>Diesel</b>
Octane/cetane number	120-130	85-95	45-55
Molar mass (kg/mol)	17.3	109	204
Stoichiometric (A/F) <sub>s</sub> mass	17.2	14.7	14.6
Stoichiometric mixture density (kg/m <sup>3</sup> )	1.25	1.42	1.46
Lower Heating Value (MJ/kg)	47.5	43.5	42.7
L.H.V. of stoichiometric mixture (MJ/kg)	2.62	2.85	2.75
Combustion energy (MJ/m <sup>3</sup> )	24.6	42.7	36
Flammability limit in air (vol% in air)	4.3-15.2	1.4-7.6	1-6
Flame propagation speed (m/s)	0.41	0.5	-
Adiabatic flame temperature (°C)	1890	2150	2054
Auto-ignition temperature(°C)	540	258	316
Wobbe index (MJ/m <sup>3</sup> )	51-58	-	-

## **2.3 Type of injection system**

The fuel injection types used in newer cars include four basic types:

### **2.3.1 Single-point or throttle-body injection**

The earliest and simplest type of fuel injection system ever made. Single-point injection simply replaces the carburettor with one or two fuel-injector nozzles in the throttle body known as the throat of the engine's air intake manifold. Single-point injection was a stepping stone to the more complex fuel injection system. Even though TBI is not as precise as newer systems, TBI meter fuel is better control than a carburettor and is less expensive and easier to service.

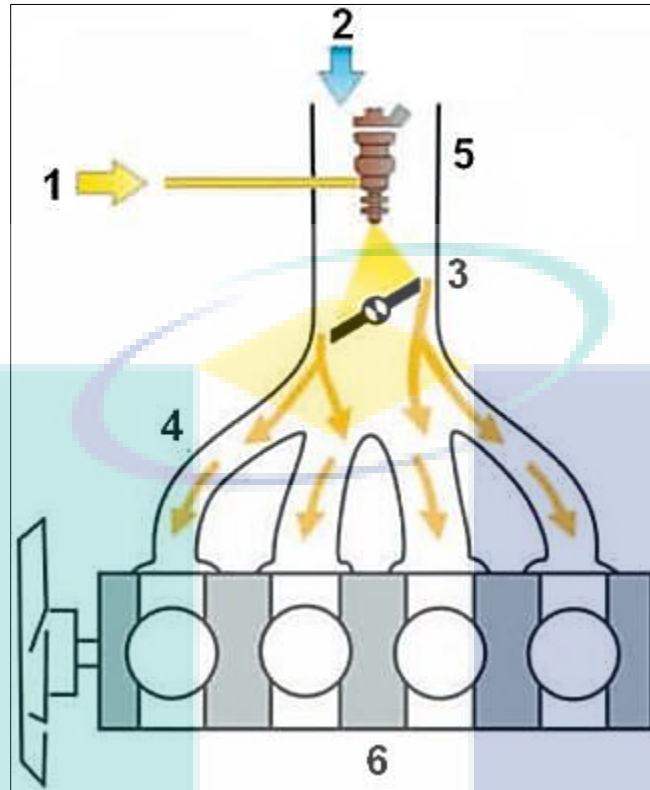


**Figure 1: Single point/throttle body injection system**

### **2.3.2 Port or multipoint fuel injection**

Multipoint fuel injection assigns an injector nozzle to each cylinder, right outside its intake port, which makes the system sometimes called port injection. Blasting the fuel this close to the intake port almost ensures that it will be drawn completely into the cylinder. The main advantage is MPFI meters fuel more precisely than TBI designs, achieving the better desired air-fuel ratio and improving all related aspects. Also, it virtually eliminates the possibility that fuel will condense or collect in the intake manifold. TBI and carburettor intake manifold must be designed to conduct the engine's heat. This is proven unnecessary on MPFI engines, thus the intake manifold can be formed from lighter-weight material. As the result, fuel-economy therefore improved. Also, where conventional metal intake manifolds must be located atop the engine to conduct heat, those used in MPFI can be placed more creatively, granting engineers design flexibility.

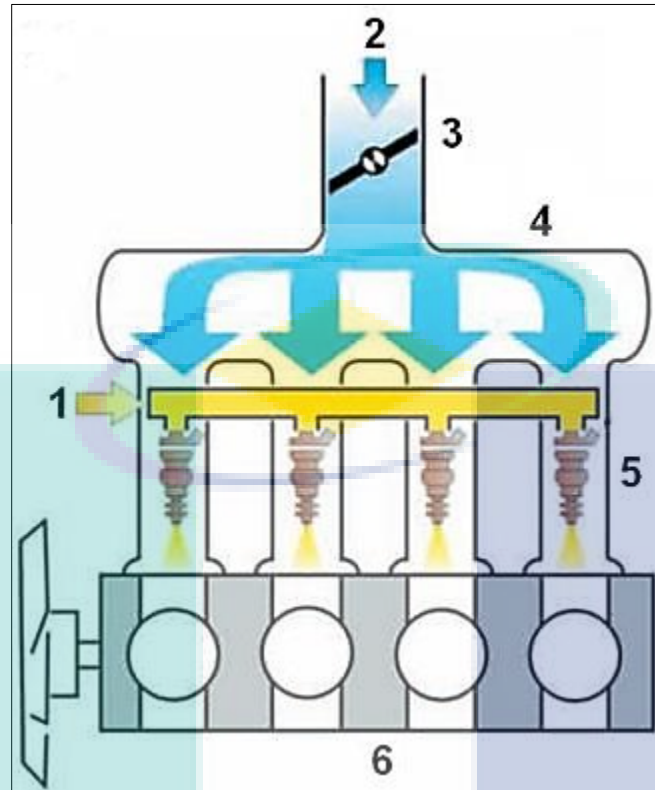


**Figure 2: Multi point/port injection system**

### ***2.3.3 Sequential fuel injection***

Sequential fuel injection, also known as sequential port fuel injection (SPFI) or timed injection is rather a type of multiport injection. The basic MPFI operates multiple injectors, but the fuel is sprayed from each injector all at the same time. As a result, the fuel may reside in a port for as long as 150 milliseconds when the engine is idling. Sequential fuel injection triggers each injector nozzle independently. Timed like spark plugs, they spray the fuel immediately before or as their intake valve opens. It improves the efficiency and emissions.

### ***2.3.4 Direct injection***

Direct injection is the latest fuel injection concept, injecting fuel directly into the combustion chambers. It is more common in diesel engines, direct injection is starting to integrate in gasoline engine designs were sometimes would call GDI for gasoline direct injection. Again, fuel metering is even more

precise than in the other injection systems, and the direct injection gives engineers yet another variable to influence precisely how combustion occurs in the cylinders. The science of engine design scrutinizes how the air-fuel mixture swirls around in the cylinders and how the explosion travels from the ignition point. Things such as the shape of cylinders and pistons; port and spark plug locations; timing, duration and intensity of the spark; and number of spark plugs per cylinder all affect how evenly and completely fuel combusts in a gasoline engine. Direct injection system is another one that can be used in low-emissions lean-burn engines.

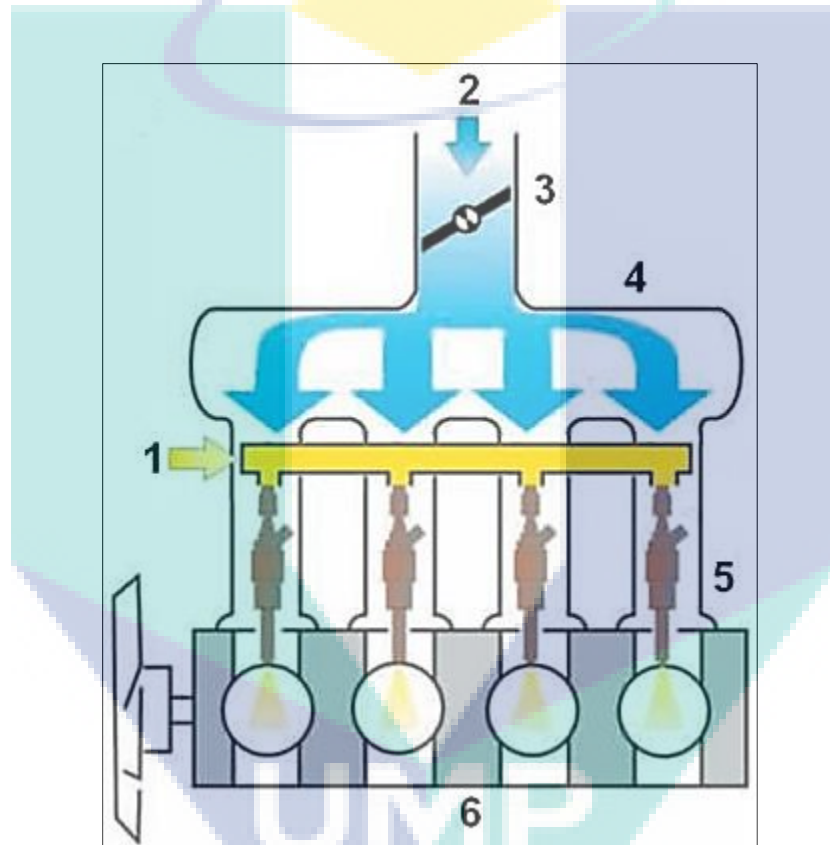


**Figure 3: Direct injection system**

Previous studies have concluded that the power loss of CNG engine can be compensated by the use of direct injection CNG fuel system [1], [13]. The characteristics of direct injection CNG affect the overall engine performance. Therefore it is very crucial to investigate the injection characteristics, fuel metering, design and optimization of such system. Hence, this study is conducted to analyze the fuel metering of direct injector used for CNG fuelling.

## 2.4 Injector for CNG

Commercialized CNG direct injectors are hardly found in the market. Thus a commercial GDI injector is used to inject CNG. Based on the previous study, it can be seen that peoples have been using outward opening poppet valve injector for CNG experimental testing [14, 15, 16, 17,18] but in [6] they clearly stated the fuel injector they used; a commercial HDEV 5 Bosch single hole gasoline direct injector. The changes of fuel properties from gases to liquid affect the injector characteristic benchmarked by the manufacturer. This is the utmost important reason on why the injector characterization for natural gas engine is highly desirable. Conventional fuel injectors are mostly used solenoid drive unit. The electrical energy is converted to mechanical energy in term of pintle displacement via electromagnetic principle. The movement of the pintle defines the opening and closing of the nozzle which in fact controlled the fuel flow through the nozzle.

The linear displacement of injector's pintle is an important variable for injector control. However, the physics involved in fuel injector operation is an interaction of electromagnetic, mechanical dynamic and fluid dynamic. The displacement occurs only when the magnetic force overcomes the opposing forces. A high performance injector required the pintle dynamics to have the following characteristics:

1. Quick response,
2. Repeatability,
3. Least power consumption [5].

Short opening delay and short closing delay are characteristics of a quick response injector. The opening and closing delay affect the minimum total time for injection duration and injection timing. Actual mass injected in very short injection duration might not resemble theoretical values. This is because the pintle needs to open and close at a higher frequency. Current of the injector also affects the pintle response. Insufficient current supply may cause the pintle to partially pulled and vibrated during the opening and closing of the injector. Moreover, higher current would create more heat in solenoid, which increases the temperature of the surrounding magnetic material. These have become another factor that will affect the pintle response time such as hydraulic hysteresis, magnetization hysteresis and saturation of the magnetic material.



## 2.5 Mass flow rate

The losses are suspected as the major cause for fluctuating injector mass flow rate. The fluctuating mass flow rate affects the engine torque stability. To study mass flow rate of the injector, instantaneous mass flow rate need to be record. However, for the mass flow rate to be accurately record we have use mass flow meter sensor which is very costly and hard to get hold of one. So, a simpler approach and option needs to be taken into consideration. The suggested solution was to switch mass flow meter with laser sensor. The laser sensor can measure the displacement of opening and closing of the pintle of injector. The displacement reading can be said to directly proportional to mass flow rate reading.

## 2.6 Driver and controller

### 2.6.1 Saturated driver (high impedance)

There are two types of drivers in injection systems. One is the saturated driver, and another one is the peak and hold driver. Injector operating parameters need to match with the ECU. Most domestic production Electronic Fuel Injection (EFI) systems use an ECU with 12 volt Saturated Circuit drivers. These systems are very inexpensive, simple, and reliable. The driver works by supplying 12 V to the injectors and the ECU turns it on and off to establish a fuel injector pulse. In general, if an injector has a high resistance specification (12-16  $\Omega$ ) the ECU uses a 12 V saturated circuit driver to control it. This means that the current flow in the driver and injector circuit stays low keeping the components cool for long life while operate at low current levels (0.8-1 A). The downside to a Saturated Circuit driver is that it has a slower response time (opening and closing time) sacrificing dynamic range. This slower time can somewhat decrease the usable operating range of the injector energized by this driver. Ohm's law ( $V=IR$ ) can be used to show the relationship between injector resistance and current level, where  $V$ =Voltage,  $I$ =Current (amps) and  $R$ =Resistance (ohms). A high impedance injector (14  $\Omega$ ) used in a 12 V system would require an operating current of 0.86 A.

$$I = \frac{12V}{14\Omega} = 0.86 A \quad (1)$$

An injector operating on a saturated circuit driver typically has a reaction time of 2 ms while a peak and hold driver typically responds in 1.5 ms.

### 2.6.2 Peak and hold driver (low impedance/current regulated)

The next kind of driver is called Peak and Hold Drivers and Injectors. These types of injectors and drivers may also be called current sensing or current limiting. Peak and Hold injectors are usually used in aftermarket high performance systems. Because they are more expensive and complex than saturated circuit drivers, they are not generally used with domestic production ECUs. Most high flow injectors are low resistance (2-5  $\Omega$ ) and use a peak and hold driver to activate them. With this type of driver, 12 V is still delivered to the injector, but because of its low resistance, the current in the driver circuit is high. The substantial increase in current flow is something a saturated injector cannot handle. The Peak current quickly opens the injector while the lower Hold current rating is used to keep it open for the duration of the ECU command. Because these injectors have larger physical parts and often work against high fuel pressure, they require an extra juice from the higher current to keep the opening and closing time of the injector stable at the higher fuel flow rate.

A peak-and-hold driver circuit utilizes fuel injectors with low resistance coils (2-2.5  $\Omega$ ) which require more current (4-5 A) to open; Ohm's law:

$$I = \frac{12\text{ V}}{2.5\ \Omega} = 4.8\text{ A} \quad (2)$$

The driver circuitry will overheat if the injector is constantly operated at 4 A. Therefore, a switching mechanism is built into the circuit which will turn down the current to a lower, more acceptable level after the injector is opened. Once the injector is opened, it takes far less current to keep it open. After the initial peak of 4 A is reached, the driver turns down the current to 1 A which holds the injector open for the duration of the pulse width. The advantage of this system is the quick response time of the injector. The high initial current instantly creates the magnetic force require to raise the valve. This allows for a wide dynamic range.

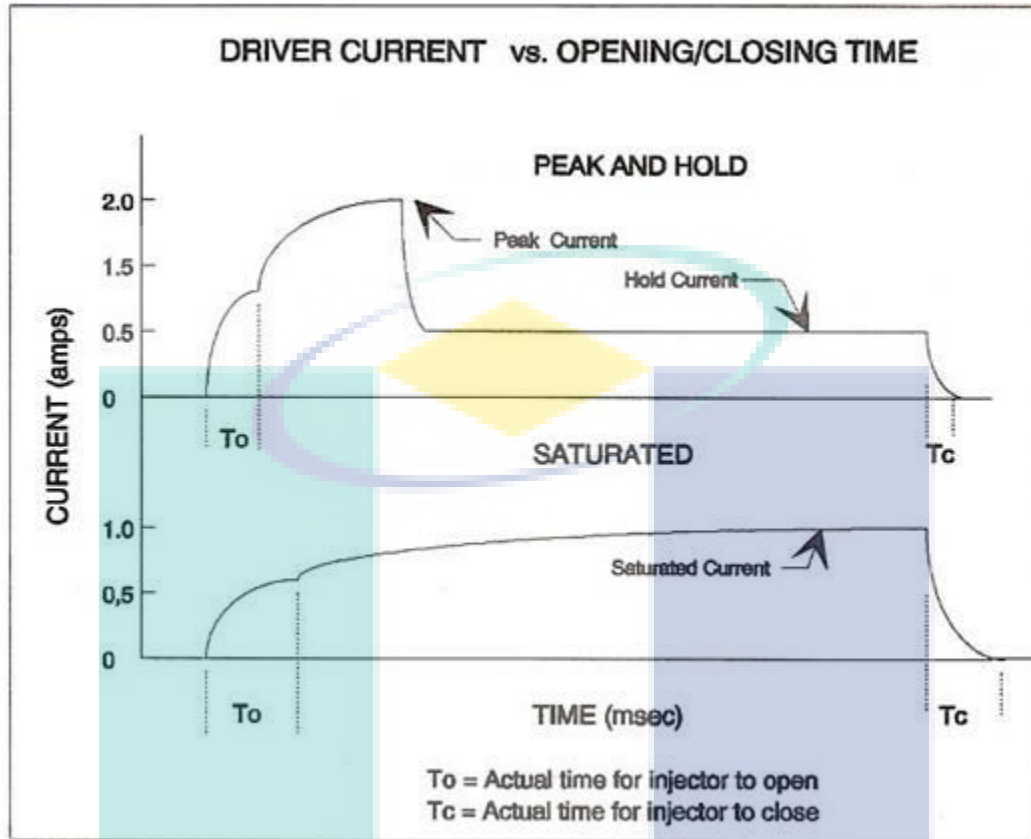


**Figure 4: Comparison between peak and hold driver with saturated driver**

Figure 4 shows the relationship of current and opening times for high and low impedance fuel injectors. It is not recommended to use low resistance injectors in a saturated driver circuit as the additional amperage required to open the injector can overheat the ECU causing permanent damage. The injector opening and closing times may become unstable thus, creating rough engine operation and possible lean misfires. Although, it is possible to install high resistance injectors in a peak-and-hold system since the amperage needed to open the high resistance injector is lower and within the limits of the peak-and-hold driver circuit.

Important observation of the direct injector operation regardless of diesel, gasoline or gaseous fuel application, they are based on current-drive solenoid [4]. This is due to the fact that the high current is used to generate high electromotive force to overcome resistance force. The resistance forces are mostly

dominated by the static spring load and the high fuel injection pressure which is common in direct injection application. In practical, in order to increase electromagnetic force, the current of solenoid coil must be increased. The direct injectors are mostly based on peak and hold current injection system. A high current pulse is given to increase the electromagnetic force by providing a short pulse of peak voltage. This can boost the opening speed, and then decreasing drive current to hold current, which is lower than peak current. At this moment, the high-speed solenoid valve is kept in maximum opening position [4].

Benefits of current-drive injectors are described by Huang et. al; At the beginning, peak current is as high as it can to quickly open solenoid valve. At hold current stage, the current is low enough to fast close solenoid valve, besides, lower hold current can protect solenoid valve coil. In this way, current-drive injectors can increase response speed of the solenoid valve to effectively control dynamic flow range. Furthermore, temporal and spatial distribution of gas and fuel mixture is easier to control. The supply voltage should be high, to provide a large current to overcome the spring preload and quickly accelerate the needle to its full open position. In addition, the large current is only required during the initial opening of the injector, and should return to nominal values to protect the solenoid from overheating.

## **2.7 Injector testing**

Static and dynamic testing of the injector using stock/ standard/ existing injector driver and controller are conduct. The “no fuel test” is referring to the dynamic injector test which is used to characterize the dynamic response and the “with fuel” test condition is referring to the static test which is use for flow characterization. The static test of the injector is used to determine the mass flow rate of the injector [2]. Recent study carried out with the existing in house facility shown that the averaged mass flow rate possess fluctuating reading. Based on Cheng et. al [3], the most possible causes for the inconsistencies are the due to the electromagnetic or power losses.

Power losses are able to be characterized by the dynamic test which measures multiple types of current and voltage in injector operation. The current and voltage profile during coil energizing and de-energizing describe the hysteresis of the solenoid which define the power losses inside the coil [3]. Additionally, the power losses may be modelled using multi-physics approaches as the losses can be readily

defined and classified independently as its constituents namely Ohmic loss, core loss, eddy current loss, solid loss, and stranded loss. Power loss analysis for CNG/ gaseous fuel direct injector is scarcely studied.

In a recent work of Kalam and Masjuki [1], the CNG direct injection engine performance have been presented and the potential of CNG direct injection to surpass gasoline port injection performance has been demonstrated. However, no detail discussions on direct injection control have been delivered. Erfan et. al [2] have focused on the flow characterization of CNG direct injector. They had studied the structure of Compressed Natural Gas (CNG) jet which is directly injected into an optical constant volume chamber for different pressure ratios. They had also investigated the variations of mass flow rate of the injector due to the variation of injection pressure and combustion chamber pressure. Their study only concentrated on the static flow characterization and no dynamic response of the injector have been characterized and discussed. Chitsaz et. al [19] had investigated the effects of nozzle geometry and pressure ratio for a dedicated correlation of CNG–SIDI injector. It was found that higher pressure ratio and exit nozzle diameter led to more tip penetration except the initial stages of jet development. Hajjalimohammadi [20] had studied the effects of nozzle pressure ratio on the jet axial and radial penetrations and tip velocity. They had proposed an analytical model to calculate the pressure drop during transient injection using shock tube theory. Their work had improved the model existing predictions by using the shock tube pressure drop model.

## **2.8 Optimization of injector**

Previous studies demonstrated that the optimization of direct injector driver and controller are vital for optimal gasoline or diesel direct injector performance are quite common and well established such as reported by [5], [6], [21] and [22]. However, only a few studies have reported on the design and development work of dedicated driver and controller for CNG gas injector [7], [8], [23], [24], [25]. Although, the work of Lino et. al are mostly based on the port injection of CNG gases.

Numerous attempts have been made to optimize the driven strategies and geometry structure to improve solenoid valves performances as presented in the previous section. But in order to fully utilize the advantage of the GDI injector, multi-physics simulation should be carried out simultaneously in order to improve the comprehensive performances and to understand electromagnetic actuator systems in totality. The model must consider the electromagnetic and power losses simultaneously. Transient and multi-physics

simulations of coupled electromagnetic have recently been widely used in mechanical and electronic products design and optimization. Watanabe et al. [26] optimized the geometry of the magnetic circuit and developed a new injector based on dynamic electromagnetic field simulation, the dynamic response time had a great reduce compared with the conventional one.

Bircher [27] and Motoyuki [28] performed multi-physics simulations of electromagnetic micro valves for automatic dispensing in chemistry applications. In their approaches, the whole process, including the magnetic force, the movement of the plunger, the flow, and the droplet break up, was simulated. A 2D static electromagnetic field simulation based on FEM was analyzed by Hideyuki Watanabe et al. [26]. S.V. Angadi [29] used the finite element method to analyze the coupled effects of electromagnetic, thermodynamics and solid mechanics. The results predicted that the main reason of the solenoid valve failure was caused by the comprehensive stress and high temperatures of the coil. Dean Cvetkovic et al. [30] established the theoretical model for the high speed solenoid valve, and preliminary implemented the coupling of electro-magneto-mechanical. Klaus Mutschler [31] used network simulation methods for modeling of a solenoid dispensing valve based on simulation software SABER (Synopsys).

The suggested model based optimization to use in this study is rate shaping method. There are two methods of injection rate shaping control using common rail system: control using nozzle needle seat throttling and control using pressure modulation [32]. However, both methods has its own pros and cons. Control using needle seat throttling results in better atomization of spray near the nozzle exit due to increased cavitation from partial needle opening. On the other hand, pressures modulated control shows longer penetration and smaller spray angles [33]. Seebode et al. [34] showed a comparison between needle controlled and pressure controlled injection rate shaping effect on engine performance and emission.

## METHODOLOGY

### 3.1 Introduction

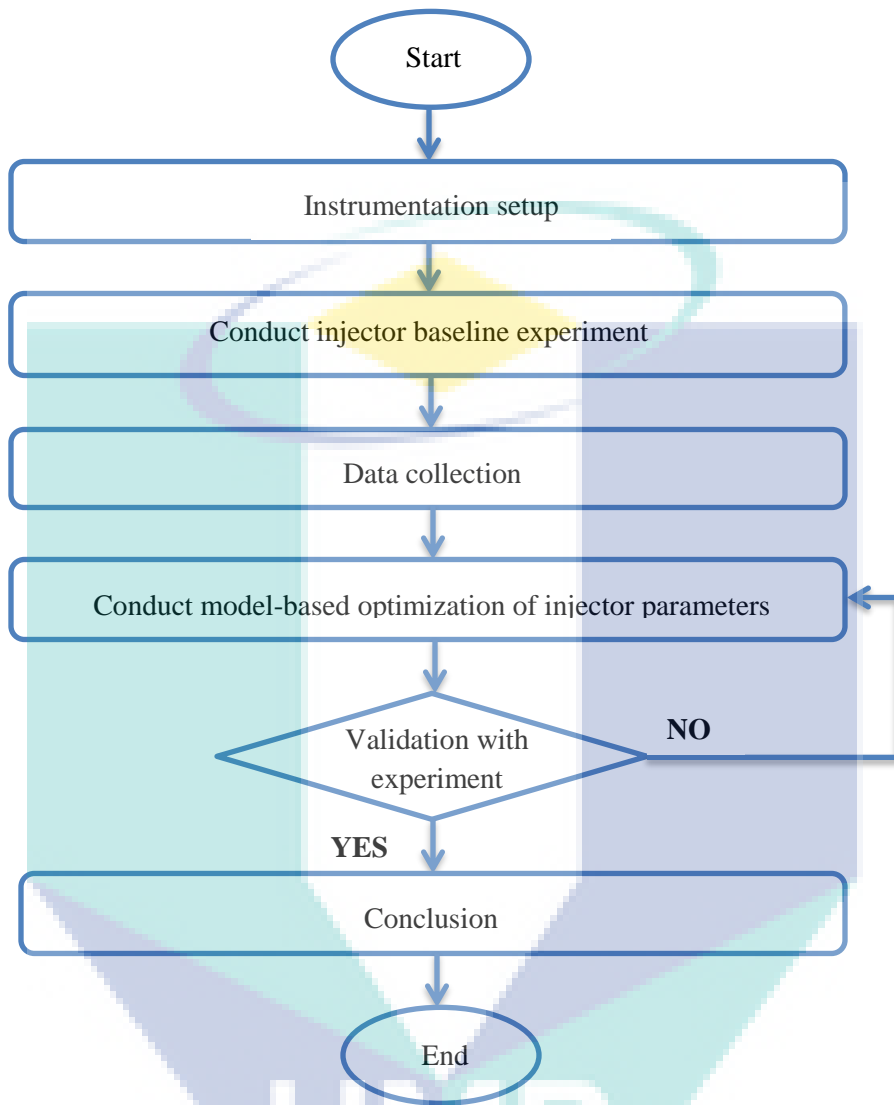
In this part, methodology is one of the processes or method that will describe more about the flow that will be taken throughout the project that already been summarized. In this chapter the method will briefly discuss based on how the test rig will be constructed, the testing procedure and how the data will be taken from the experiment to be analyse. The method that will be used in developing the project is by referring to the flow chart that had been decided. This has helped in giving the project run smoothly.

### 3.2 Flowchart

The flowchart is the process flow of project from the beginning until completion. This can be a guideline to start research and problem can be detected in more effective way.



UMP





### 3.3 ANSYS Maxwell simulation

The simulation procedure for ANSYS Maxwell will be explained according to the equation use for model such power loss model and electromagnetic model. An explanation will clearly demonstrate step by step.

#### 3.3.1 Power losses model

The solenoid injector's power losses have many different forms, including ohmic loss, core loss, eddy current loss, solid loss, stranded loss, etc. All these power losses are associated with the ultra-high-speed solenoid injector performance.[3]. The Ohmic loss is caused by a conductor's current distribution of conduction. The power loss for Ohmic loss is related to the conductor's resistivity when the conductor's current flow. It is also known as the effect of Joule-Lenz. Because of the Ohmic loss and known as Joule heating, there is always a thermal effect. The Ohmic loss equation is provided:

$$P_{ohmicloss} = \int J \cdot J^* \cdot \sigma^{-1} \cdot dV \quad (3)$$

$J$  = current density

$J^*$  = complex conjugate of the current density

$\sigma^{-1}$  = conductivity

Next, for only a transient solution type core loss combines eddy current losses with hysteresis losses. It is an analysis based on transient magnetic field density already measured after processing. It shall apply to the evaluation of core losses in steel laminations often used in applications such as electrical machines, transformers or power ferrites. The equation as follow:

$$P_{core} = P_h + P_c + P_e \quad (4)$$

Where;

$P_h$  : hysteresis loss

$P_c$  : eddy current loss

$P_e$  : excessive current loss

The hysteresis loss, eddy current loss and excessive loss equation as follow:

$$P_c = k_c(fBm)^2 \quad (5)$$

$$P_h = khfB^2m \quad (6)$$

$$P_e = k_e(fBm)^{1.5} \quad (7)$$

Where;

- $k_c$  : classic eddy current loss coefficient
- $kh$  : loss of hysteresis
- $B$  : excessive loss
- $f$  : the frequency of the driven signal
- $m$  : the magnetic induction intensity amplitude

Next, the solid loss and stranded loss both have use same equation which is represent the resistive loss in the conductor when current pass through it. The different is each equation has own purpose The solid loss for solid conductors while using stranded loss for stranded voltage using external circuits. The equation as follows:

$$P_{solidloss} = 1\sigma \int \Omega^2 \cdot dvol \quad (8)$$

Where;

- $\Omega$  : the conductivity of the material

### 3.3.2 Electromagnetic and Mechanical losses model

The major forces on movement components are electromagnetic force, spring preload force, fuel hydraulic force and gravity. Newton's dynamic balance equations, which include fluid-dynamic force, spring force and gravity, and electromagnetic forces, can thus describe the cinematic equation. The expression as follow:

$$F_m - F_{sp} - F_{flu} - mg = md^2x/dt^2 \quad (9)$$

Where;

$F_m$  : magnetic force

$F_{sp}$  : spring preload force

$F_{flu}$  : hydraulic force

$m$  : armature mass

$g$  : gravity,  $9.81 \text{ kg/s}^2$

$x$  : solenoid valve displacement

The positive direction is described as the armature near the core.[3] The electrical behaviour of solenoid injector can be applied using Kirchoff's law equation. The equation as follow:

$$V - Nd\phi/dt - Ri = 0 \quad (10)$$

Where:

$R$  : resistance of the solenoid coil

$i$  : electrical current

$V$  : voltage

$\phi$  : magnetic flux

$N$  : number turn of coil

### 3.3.3 *The injector computational domain*

The model was developed based on the assumption of symmetrical domain where only one fourth of the injector was modelled. The 2D axisymmetric model is used for models which have a high symmetry around one axis and import to the ANSYS software for simulation process.[5]

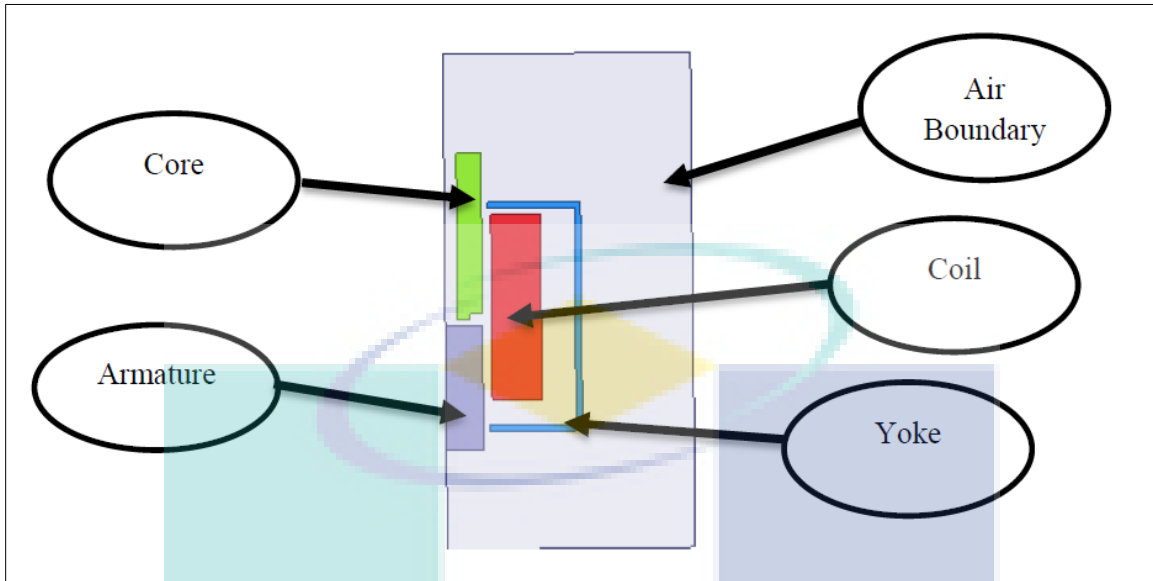


**Figure 5 : 2D model of injector**

In this project, 2D geometry model was chosen for the simulation process. Using 2D simulation, the computing of simulation will be short rather than 3D which takes more computing time to complete the simulation. For the benefit using 2D model simulation is fewer assumptions and less user judgment yield results that are representative of actual conditions. When meshing process, the number of element for 3D is higher than 2D because 2D only have flat surface and the geometry arrangement is balance while 3D has solid surface and irregular in geometry shape. For this type of project both simulations can done either 2D and 3D, the result will be almost same for both simulation. This has been proven by ANSYS Maxwell user that research on the core loss produce the transformer. He make the comparison on single phase transformer analysis which both simulations give almost same result value and the different is completing time for simulation.

### 3.3.4 Electromagnetic simulation procedure

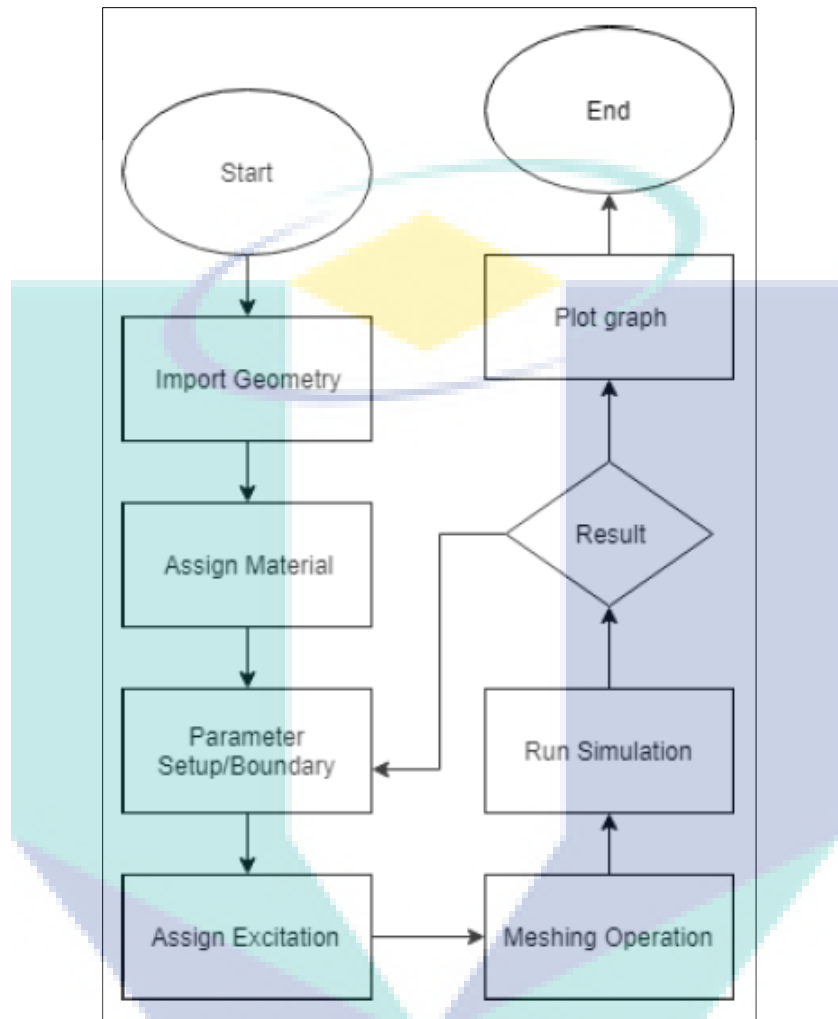


**Figure 6 : Simulation Flow Chart**

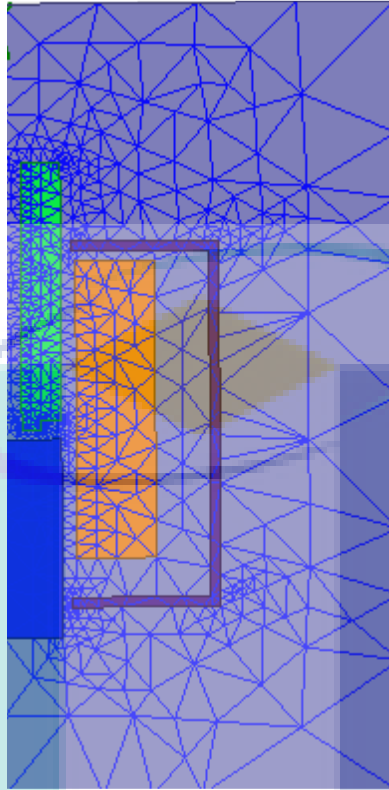


**Figure 7 : Simulation 2D meshing**

**Table 3 : Simulation Parameter**

<b>Parameter</b>	<b>Value</b>
Voltage	12 v
Frequency	500Hz
Coil Turn	160
Resistance	1.5

This parameter use for simulation is according the real experiment parameter. In order to compare result, the result must validation with the real injector testing result. The simulation result must less than 10% different with the real result exceed than 10% the simulation result will be error. If the result recorded were not satisfied or facing an error, the parameter is to be set again and troubleshoot the simulation whether there are incomplete boundary condition, parameter and etc.

### 3.3.5 Maxwell circuit editor procedure

The Maxwell circuit editor is used to create an external circuit. This external circuit was used to generate input to the simulation model. The advantage of this software is it can create the external circuit that can control voltage input or other input.

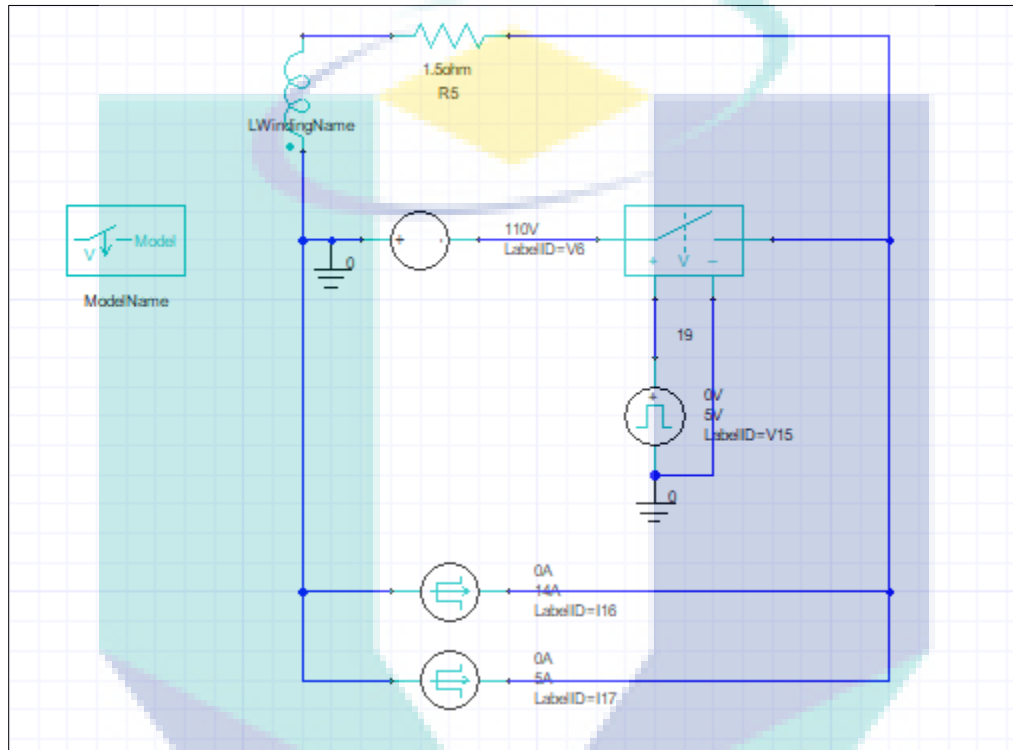


Figure 8 : Injector circuit [5]

### 3.4 Square wave experimental study

The experimental approach was used to investigate the effect of converting liquid injector into a gaseous injector. This study is a continuation of the previous analysis presented in [12] where theoretical modelling had been presented. As the type of fuel running into the injector has been changed, it was assumed that the overall operating system of the injector would be affected. Table 4 shows the summary of each case study.

**Table 4 : Square wave case study summarisation**

	<b>Controlled parameter</b>	<b>Fixed parameter</b>	<b>Significant of each case</b>
<b>Case 1</b>	Injection pressure: 20 - 60 bar.	Injection duration: 24 ms, Injection counts: 1000. Injection frequency: 1000 RPM.	To determine the effect of injection pressure on the injector mass flow rate.
<b>Case 2</b>	Injection duration: 2 - 24 ms.	Injection pressure: 50 bar, Injection counts: 1000, Injection frequency: 2000 - 5000 RPM.	To determine the effect of injection load on the injector mass flow rate.
<b>Case 3</b>	Injection frequency: 2000 - 5000 RPM.	Injection pressure: 50 bar, Injection counts: 1000, Injection duration: 2 - 24 ms.	To determine the effect of injection frequency on injector mass flow rate.

### 3.4.1 Injector Specification

**Table 5 : General BOSCH model HDEV 1.2 injector specification [13]**

<b>Attributes</b>	<b>Values</b>
<i>Mechanical specifications</i>	
Allowable maximum pressure (bar)	200
Volume flow rate (gasoline fuel/cm <sup>3</sup> /min) at 100 bar	30
Weight (g)	78
Length (mm)	85
<i>Electrical specifications</i>	
Resistance (Ohm)	0.9 @ 1.5
Voltage (Volt)	90 V
Allowable peak current (Amp)	20 A
<i>Operating Condition (Gasoline fuel)</i>	
Fuel Input	Axial (top feed)
Operating Temperatures (°C)	30-120
Permissible Fuel Temperatures (°C)	<80



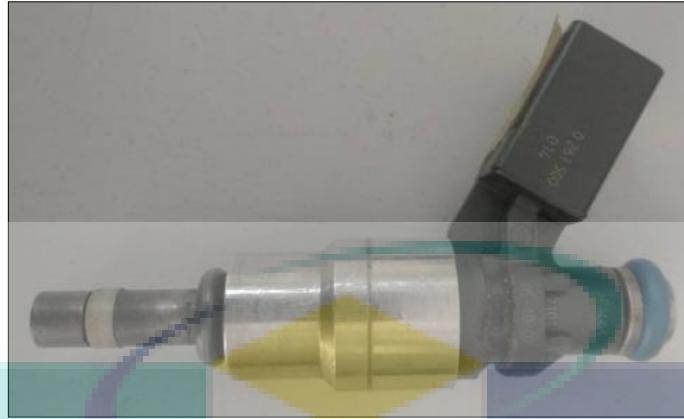


**Figure 9 : BOSCH model HDEV 1.2 injector physical appearance**

Figure 9 shows the physical appearance of the injector used in this experiment. This injector made by BOSCH with model name HDEV 1.2. The injector typically used in GDI engine. The specification of the injector is listed in Table 5 above. The injector used in this experiment is a single-hole type model. It improves the atomization of fuel as the fuel is forced into the combustion chamber to turn into fine mist.

UMP

### 3.4.2 Instrumentation setup and layout

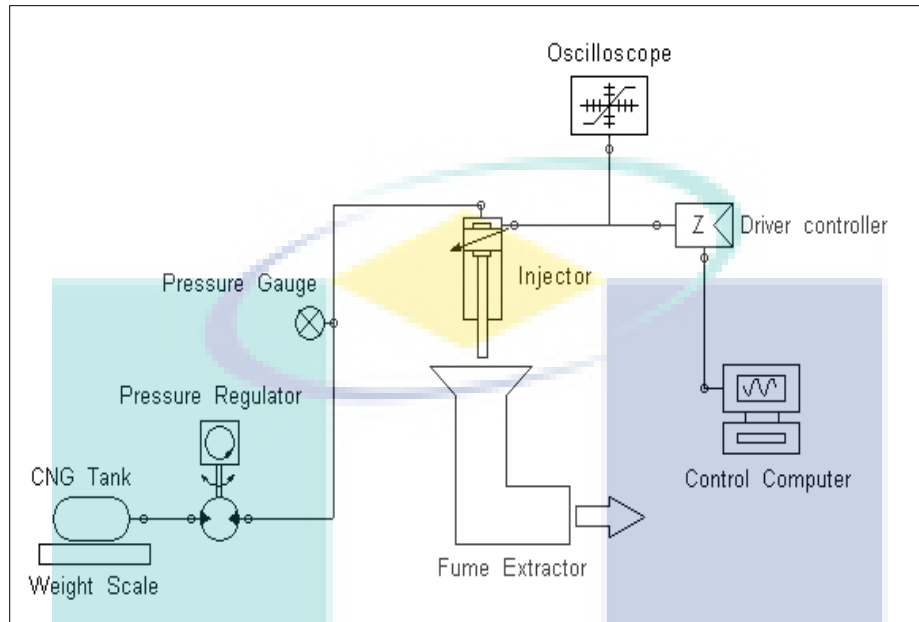


**Figure 10 : Schematic diagram of the experimental setup**

A schematic diagram of the experimental setup is presented in Figure 10. The CNG storage tank is used to supply fuel to the injector. A weighing scale is used to measure the instantaneous mass of the CNG tank. The determination of injector mass flow rate is based on the change of CNG tank mass. The CNG pressure was regulated by a pressure regulator and oversees by a pressure gauge. The PWM driver and Arduino UNO microprocessor act as an ECU to control the duration and frequency of injector. The computer was used to modify the input parameters of experimentation and send the signal to the driver and controller. Oscilloscope acted as a tool to observe and record the signal voltage produced by the injector as it operated. The actual setup of the experiment is included to show how the test being conducted.

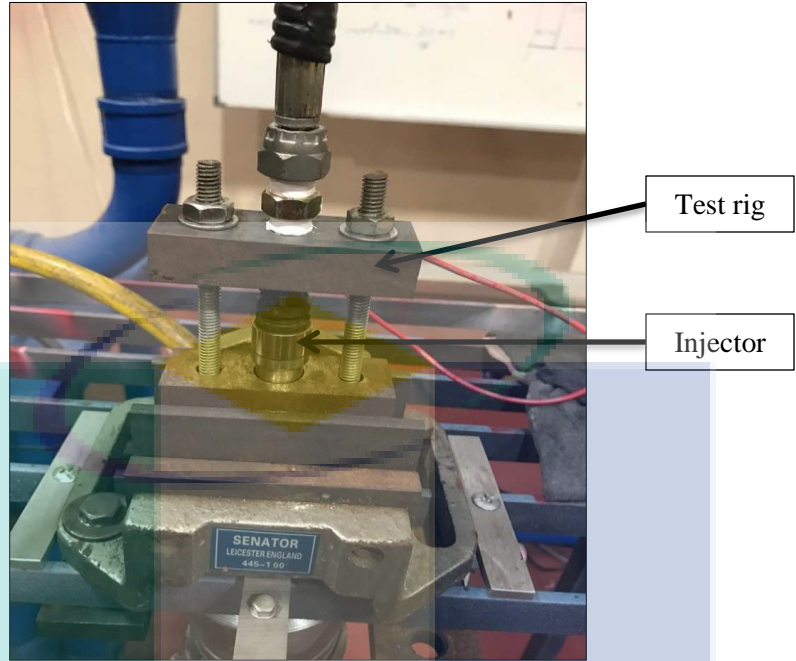


Figure 11 : The injector being clamped to the test rig

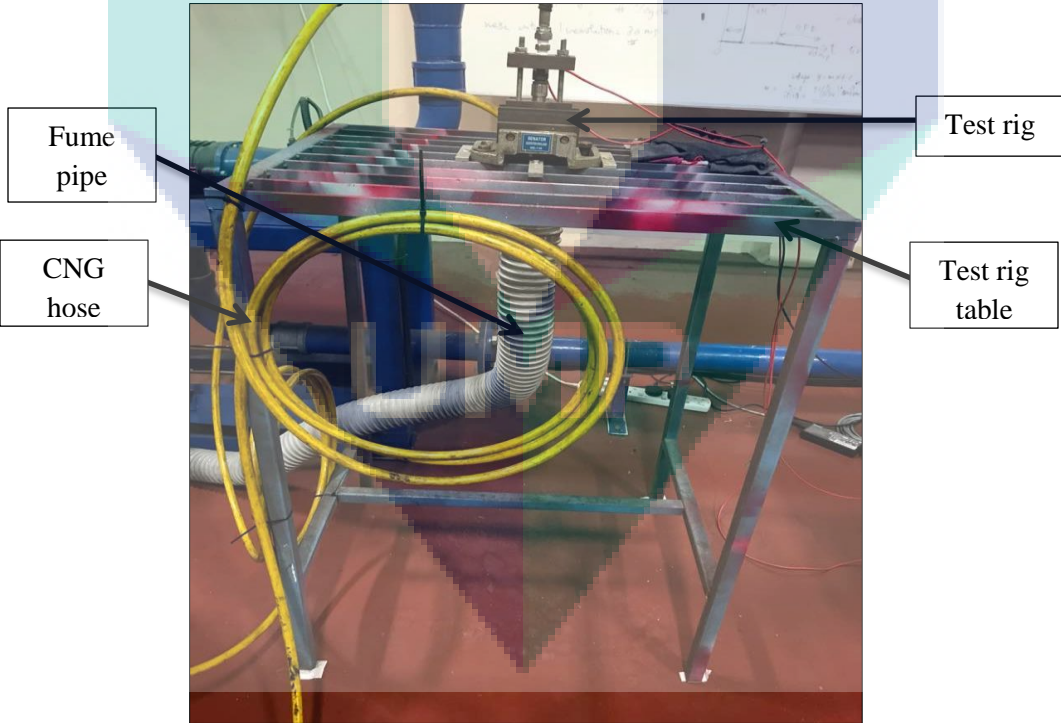
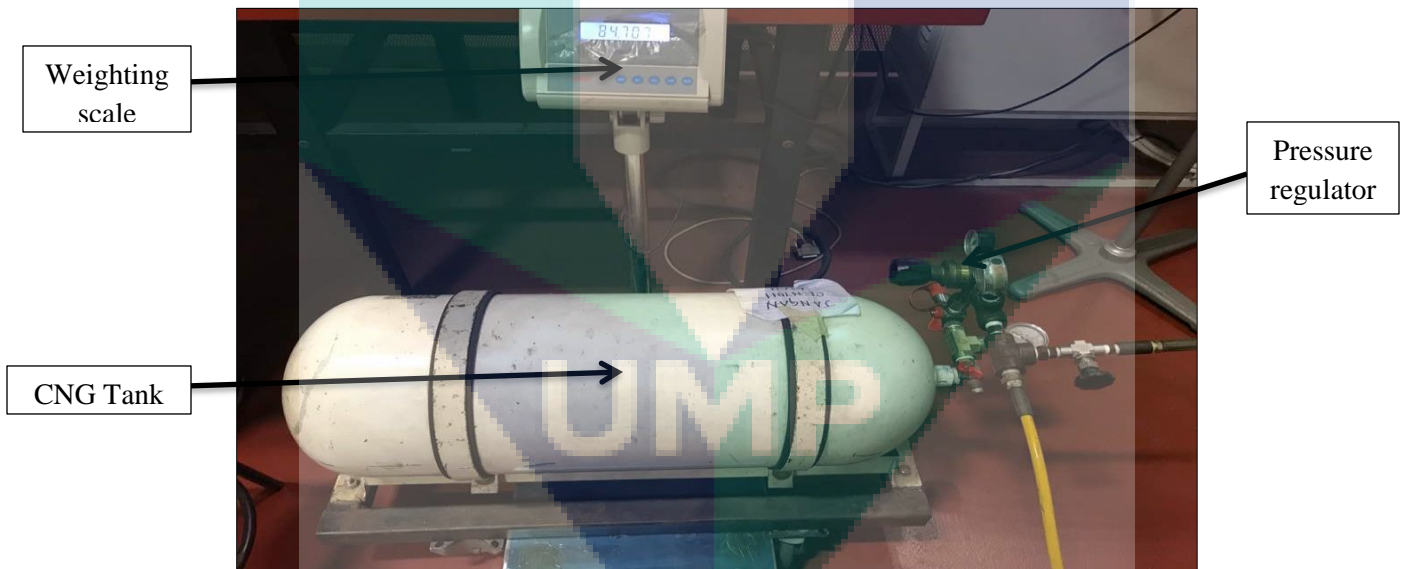


Figure 12: The custom test rig bolt on table



Fume  
extractor

**Figure 13: The fume extractor being used in the experiment**



Weighting  
scale

Pressure  
regulator

CNG Tank

**Figure 14: The CNG tank on top of the weighting scale**

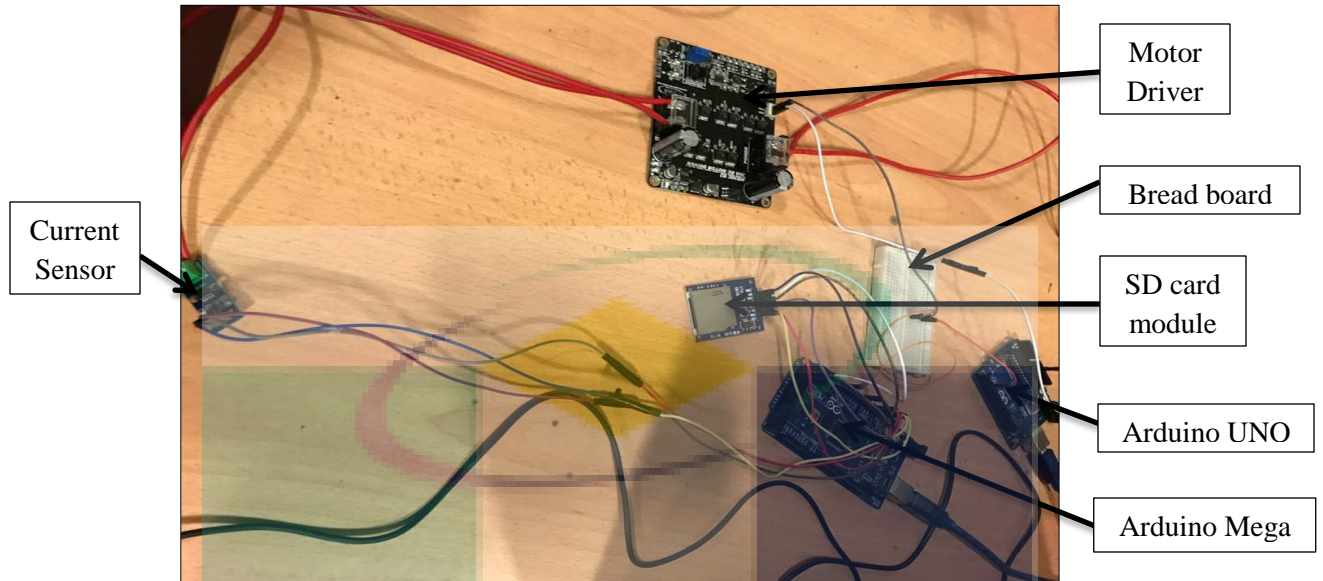


**Figure 15: The connection of driver and controller circuit for the injector**

### 3.4.3 Square wave driver and controller

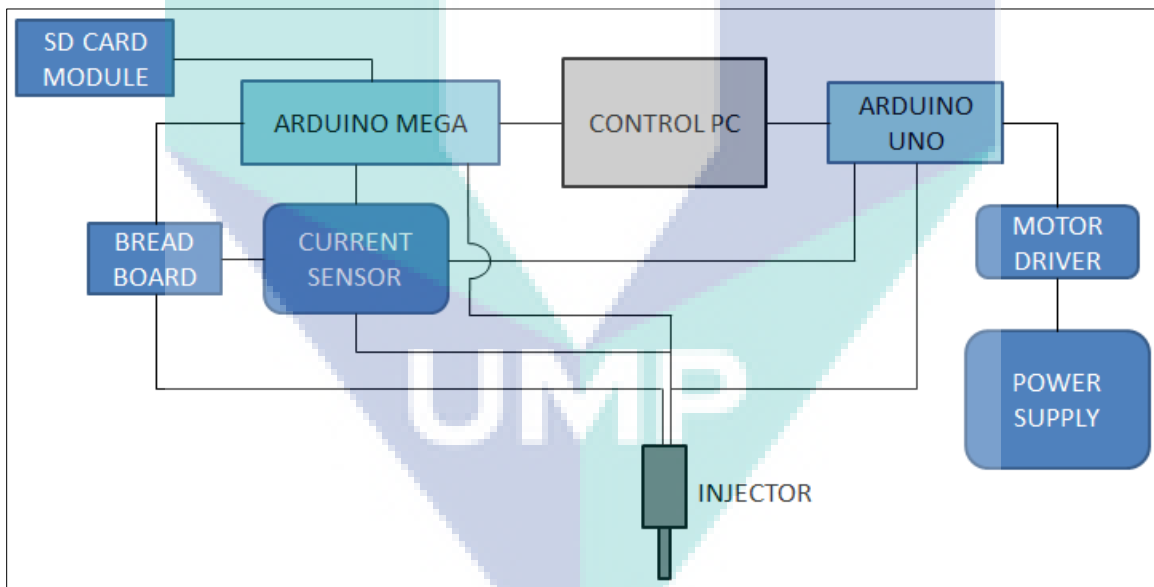


**Figure 16 : Schematic diagram for square wave driver and controller circuit**

### 3.5 Two Stage signal wave experimental study

A new proposed control strategy for fuel injector is presented and the data of injector test are collected and have been analysed. The new control strategy that produce two stage signal wave; peak and hold injector profile is used to replace a standard motor driver that just produce square wave profile in order to get a better performance of fuel injection for gaseous fuel application. The experiment was conducted using an Arduino system that connected to the actual injector system. The comparison between peak and hold profile and square wave profile was collected through the different result of mass flow rate.

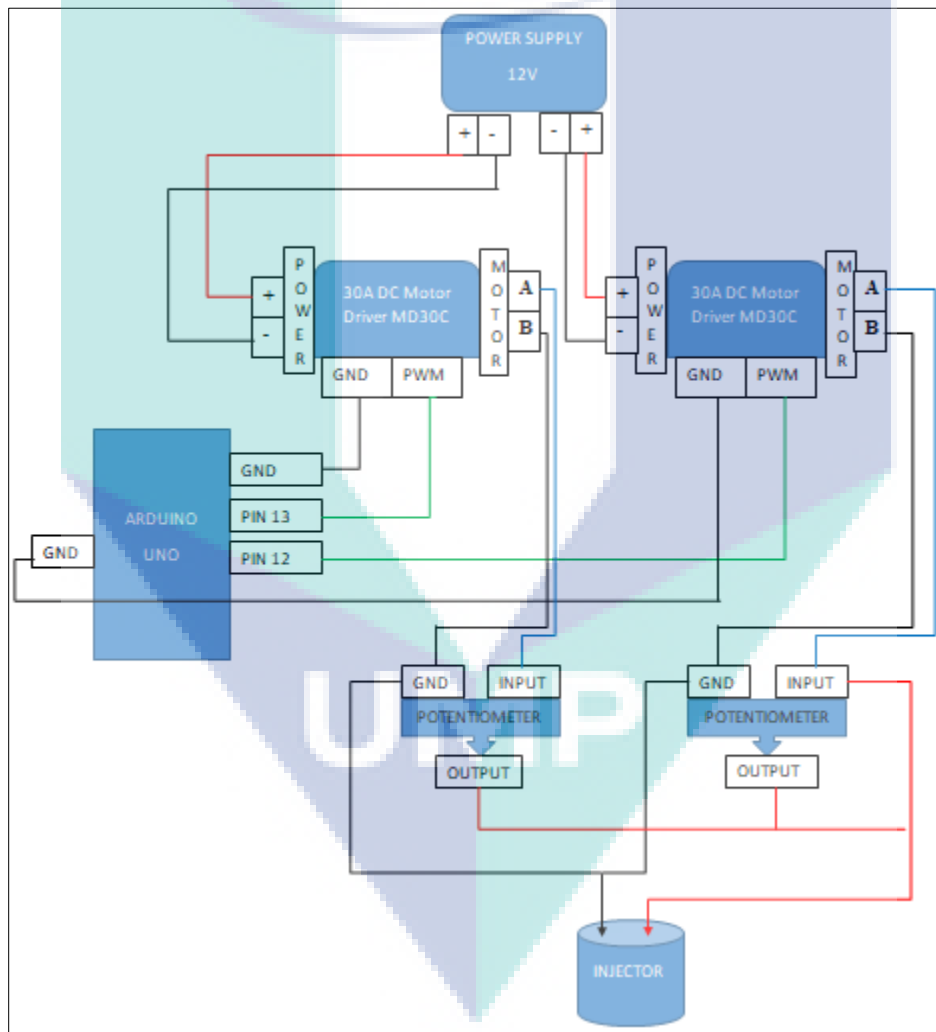


Figure 17 : Schematic diagram of two stage signal wave driver



### 3.6 Square wave simulation study

The modelling section is divided into three different section; the electromagnetic model, the mechanical model and the flow model. These models are combined and developed in MATLAB Simulink software. The Matlab ODE solver is selected as the baseline solver in the study.

#### 3.6.1 The electromagnetic model

The electromagnetic is based on the work of Schimpf [12]. The solenoid driver presented by Schimpf is a derivation of electromagnetic force regarding coil diameter, coil length, wire gauge, supply voltage, packing density, and the number of turns. This model eliminates the current term which in most cases are difficult to solve. Detail discussion and explanation of the model can be found in Schimpf. The electromagnetic force is given by the following expressions:

$$F_{mag} = \frac{-V^2 \mu_r \mu_o}{8\pi\gamma^2 l^2} \left(\frac{r_o}{r_a}\right)^2 \alpha e^{-\frac{\alpha}{l}x} \quad (11)$$

Or

$$F_{mag} = \frac{-V^2 \mu_r \mu_o}{8\pi\gamma^2 l^2} W_f \alpha e^{-\frac{\alpha}{l}x} \quad (12)$$

Where;

- $V$  : Supply voltage
- $\mu_r$  : Relative magnetic permeability of armature/pintle material
- $\mu_o$  : Air gaps magnetic permeability
- $r_o$  : Inner radius of coil cross section
- $r_a$  : Average radius of coil cross section
- $\gamma$  : Ratio of coil material resistivity to coil wire cross section area
- $W_f$  : Winding factor, equal to square of  $\frac{r_o}{r_a}$  ratio
- $l$  : Length of coil body

$\alpha$  : Ratio of inductance to relative permeability of armature material

$x$  : Instantaneous position of armature

To utilize the model, one needed to have detail information of the coil material. For example, the type of coil material, coil material resistivity and coil wire cross-section area. In general, the larger the coil wire cross section area, the larger the generated force. In the study, the selected coil wire is estimated to be based on AWG 43 which has a diameter of 0.07874 mm and copper type.

### 3.6.2 The mechanical model

The mechanical system of the direct injector is represented by a mass-spring-damper system. In the initial state, it was assumed that the pintle sits on the valve seats. In this initial state, a total of five forces are acting on the pintle. The gas pressure force, contact friction force, gravitational force, initial spring force, and finally normal reaction force. Figure 18 presents the free body diagram of the pintle in the study. The gas force is due to the CNG fuel pressure, the contact friction force is due to the contact between the pintle and surface of the valve seats, and the gravitational force is due to the mass of the pintle. The initial spring force is due to the compression of the spring at the initial state. Additional spring force will be generated as the pintle is pulled by the solenoids. The normal reaction force defines the existence of the lower and upper stopper of valve seats. This force is represented by the virtual spring, and damper unit which is equal and opposite direction of all other forces when the pintle rest or hit bottom and upper stopper.

The pintle act as a plunger which controls the open and close the nozzle flow area. During the opening state of the injector, the pintle will overcome all the resistant forces by withdrawing required current from the power supplies. The relationship between the all the forces is described by the mathematical expressions of the pintle's equation of motion which is given by equation 13. Based on the equation, the displacement of the pintle can be obtained by a twice integration of the acceleration. The mass considered in the equation is only the mass of moving the rigid body of the pintle.

$$m \cdot \ddot{x} = F_{sol} + F_{spring} + F_{contact\ friction} + F_{upper\ wall} + F_{bottom\ wall} + F_{pressure} \quad (13)$$

The spring compression force  $F_{spring}$  is defined as the sum of initial compression force and the force due to the additional compression during the solenoid activation. The equation for the spring compression force is given by the following expression.



$$F_{spring}(x) = F_0 + K_{spring} \cdot x \quad (14)$$

Where;

$F_0$  : The initial compression force, N

$K_{spring}$  : Spring constant, N/m

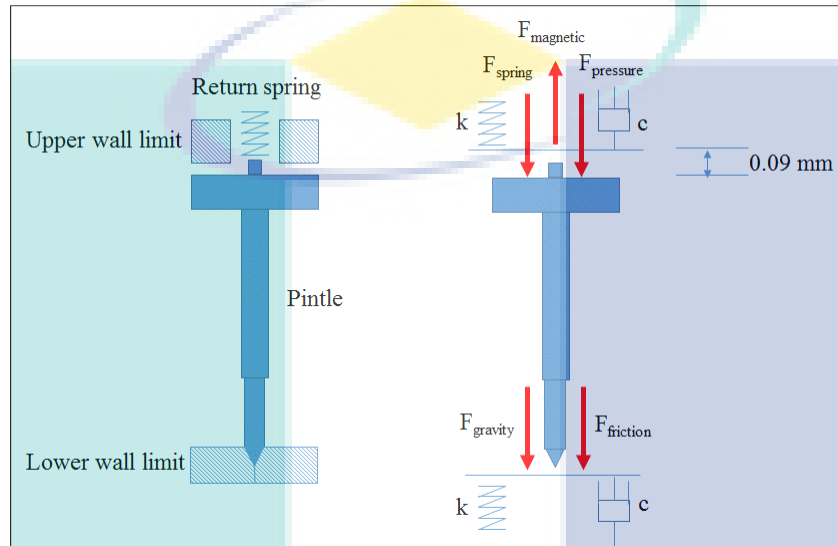


**Figure 18 : Pintle free body diagram [13]**

The initial contact friction force is given a constant value of 13.8 N at its rest position (at the upper stator or lower stator). The value will reduce to zero as the position of the pintle surpassed a threshold distance of 0.001 mm. The mathematical form of the contact friction force is given by equation 15.

$$F_{initial\ contact\ friction}(x) = \begin{cases} -13.8N, & x \leq 1e - 3mm \\ 0, & x > 1e - 3mm \end{cases} \quad (15)$$

Based on the findings of Zhang et al.[14] the displacement of the pintle is limited by the existing of the bottom and upper stator. The maximum displacement allowable for the pintle is estimated to be 0.09 mm upwardly. Farther than that, a barrier is enforced by imposing a stiff spring and damper. This is to simulate a condition where the pintle hits the stator. The reaction force imposed on the pintle at the upper wall is expressed mathematically by equation 16.

$$F_{upper\ wall}(x) = \begin{cases} -K * (x - 0.09mm) - c * \dot{x}, & x < 0 \\ 0, & x > 0 \end{cases} \quad (16)$$

As the pintle moves back to the initial position and hit the lower stator, another barrier is imposed to simulate the reaction force from the bottom stator. The mathematical expression for the lower stator reaction force is given by equation 17.

$$F_{bottom\ wall}(x) = \begin{cases} -K * x - c * \dot{x}, & x < 0 \\ 0, & x > 0 \end{cases} \quad (17)$$

Where;

$K$  : the wall stiffness, N/m

$c$  : the damping coefficient, N·s/m

### 3.6.3 The flow model

The flow model is based on one-dimensional compressible flow equation. The model considers choking and non-choke flow situations which are determined by the critical pressure ratio. Choked flow occurs when the ratio  $P_1/P_2$  exceeds the critical pressure ratio  $P_c$ , which is given by the following equation.

$$P_c = \left(\frac{\gamma+1}{2}\right)^{\frac{\gamma}{\gamma-1}} \quad (18)$$

The mass flow rate through the orifice for non-choked and choked flow conditions are given by equation 19 and 20 respectively. The only varying parameter in the equation 19 is the effective area of the nozzle which is calculated as a function of pintle displacement.

$$\dot{m} = K_{nv} A P_1 \sqrt{\frac{2M}{RT} \left(\frac{\gamma}{\gamma-1}\right) \left[ \left(\frac{P_2}{P_1}\right)^{\frac{2}{\gamma}} - \left(\frac{P_2}{P_1}\right)^{\frac{(\gamma+1)}{\gamma}} \right]} \quad (19)$$

Or

$$\dot{m} = K_{nv}AP_1\sqrt{\frac{\gamma M}{RT}\left(\frac{2\gamma}{\gamma-1}\right)^{\frac{\gamma+1}{\gamma-1}}}$$
 (20)

Where;

$K_{nv}$  : The discharge flow coefficients

$A$  : The orifice area (m<sup>2</sup>)

$P_1$  : The  $H_2$  upstream pressure (Pa)

$P_2$  : The in-cylinder pressure (Pa)

$T$  : The  $H_2$  upstream temperature (K)

The crucial part of the flow model is the definition of the nozzle effective flow area. Figure 19 presents a schematic definition of the nozzle effective flow area for the pulled-in injector. The effective flow area is defined as a surface area of a truncated cone. The effective flow area is formulated based on the work of Antunes.[15]

UMP

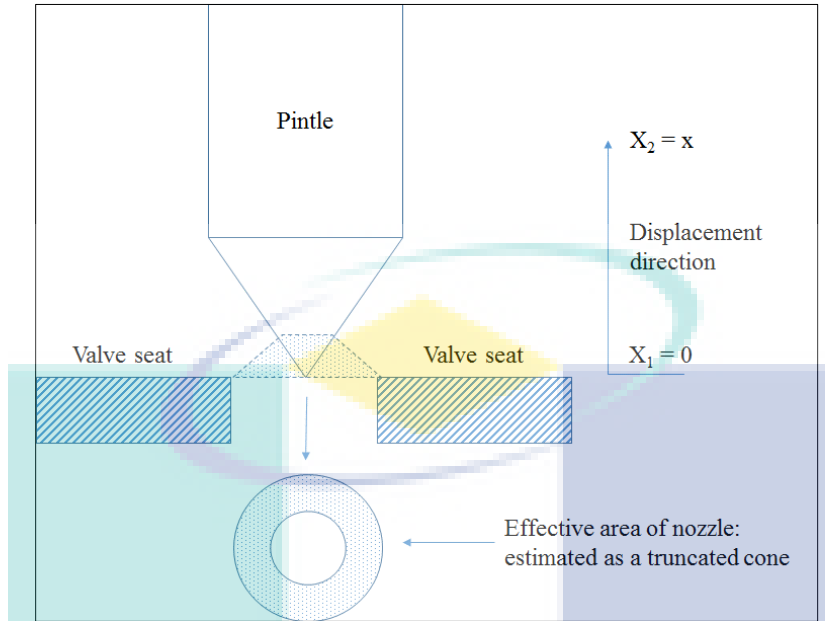


**Figure 19 : Definitions of effective flow area for nozzle flow calculation [15]**

In mathematical form, the effective area for the nozzle flow, as illustrated in Figure 19, can be calculated by using equation 21.

$$A_o = \pi \left[ \frac{(R\sqrt{R^2 + (R \sin \phi)}) - (R - X \sin \phi \sin \phi)}{\sqrt{(R - X \sin \phi \sin \phi)^2 + (R \tan \phi - X \sin^2 \phi)^2}} \right] \quad (21)$$

Where;

$R$  : The nozzle hole radius (m)

$\theta$  : The needle tip angle (rad)

$\phi$  : Equal to  $\theta/2$

The maximum area of the nozzle is given by:

$$A_{o\ Max} = \pi R^2 \quad (22)$$

### 3.6.4 The simulation setup

The simulation was carried out to replicate the two cases from the experiment for validation. A significant amount of inputs are required to ensure the model can predict as close as possible to the measured data. The general specification for the injector is followed to make sure the simulation model is not out of the course while Table 6 listed all the general and specific inputs required by the model. The electro-magnetic inputs, as well as the mechanical inputs parameter of the injector, are mostly based on Zhang et al.[14]. Figure 10 presents the schematic layout of the experimental work which is use as a reference to develop the layout of the simulation model in MATLAB Simulink shows by Figure 20. The pulse generator produced square wave signal which represents the output of the PWM driver.

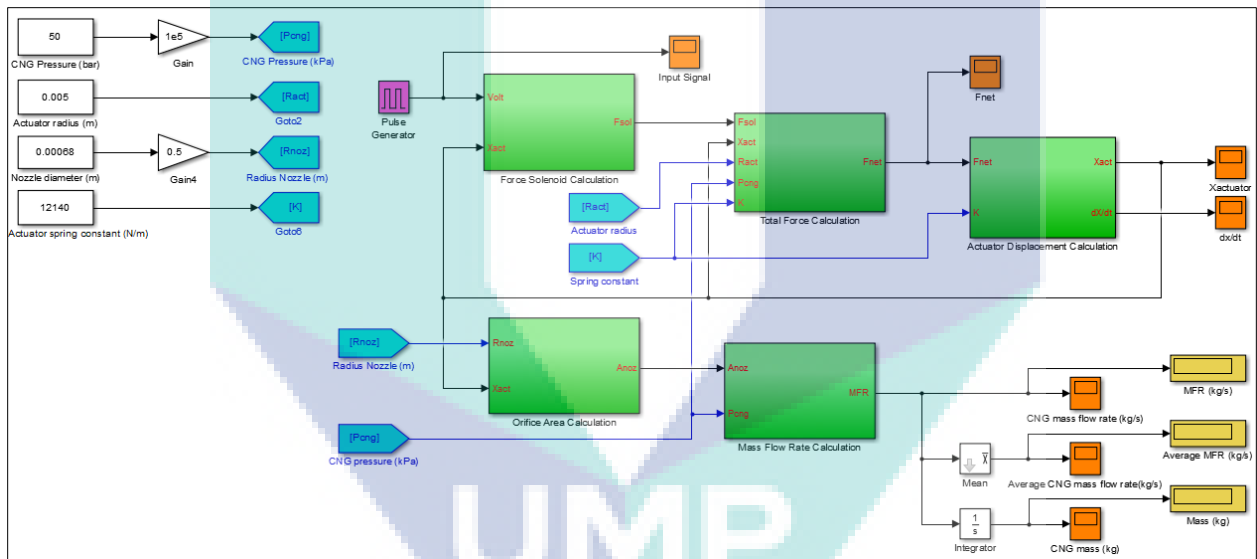


Figure 20 : MATLAB Simulink block diagrams of the injector simulation model

Table 6 : Simulation setup

Attributes	Values
<i>General Input Parameter (unit)</i>	
Actuator radius (m)	0.005

Gas pressure (bar)	50
Nozzle Diameter(m)	0.00068
Spring Constant (N/m)	12140 N/m

*Electro-magnetic Input Parameters (unit)*

Length of air gap (m)	0.00009
Magnetic Permeability of Air (H/m)	$1.256 \times 10^{-6}$
Magnetic Permeability of Steel (H/m)	3290
Magnetic circuit length (m)	~0.001
Number of Turns	160
Coil Resistance (Ohm)	0.9
Resistance (ohm)	1.5 (Zhang)[14]
Inductance (mH)	1.9 mH @ 1kHz 3.9 mH @0.12 kHz
Voltage (Volt)	90
Peak Current (Amps)	20

*Mechanical Input Parameters (unit)*

Static Spring Force (N)	40
Spring mass (kg)	0.001
Actuator Mass (kg)	0.003
Actuator Damping Constant (Nm/s <sup>2</sup> )	14.97 N.s/m
Overall Weight (kg)	0.078

*Flow Input Parameters (unit)*

Gas specific heat ratio	1.32
-------------------------	------

Gas valve flow co-efficient	0.65
Universal gas constant (J/kg.K)	8314
Gas Molecular Mass (kg/kmol)	16.04
Gas Supply Temperature (K)	300

### 3.7 Two stage signal wave simulation study

This simulation is to justify selection of 6 different input signal that can be used in Bosch HDEV 1.2 injector. The signals are taken from previous study and experiment. The injector parameter is identifying to make sure the signal can be use according to futures characteristic. In this simulation, the highest voltage used is 12V at 25ms. After all the parameter are set, validate the injector model whether it is suitable or not when using that kind of signal. Compare the simulation result with previous study and experiment to make sure the injector can operate smoothly while doing the experiment. If the signal is not suitable for the injector, it should be refining the injector model to get the best signal. Square wave signal are used as a references to modify the other 6 signals before it is test into the model.

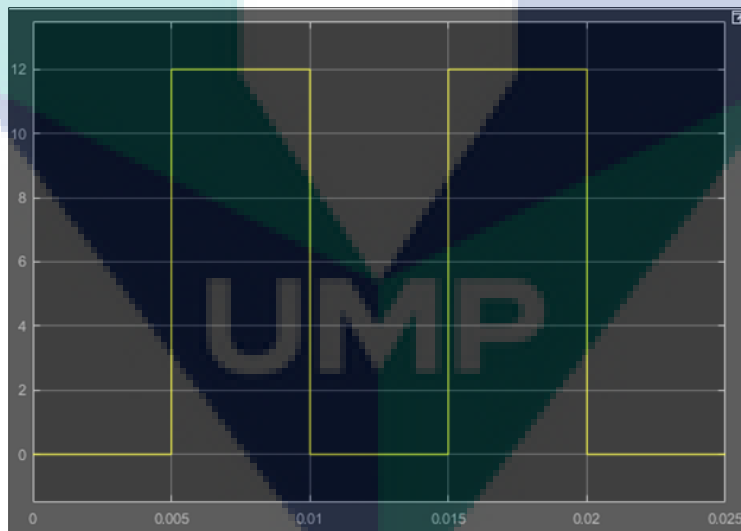
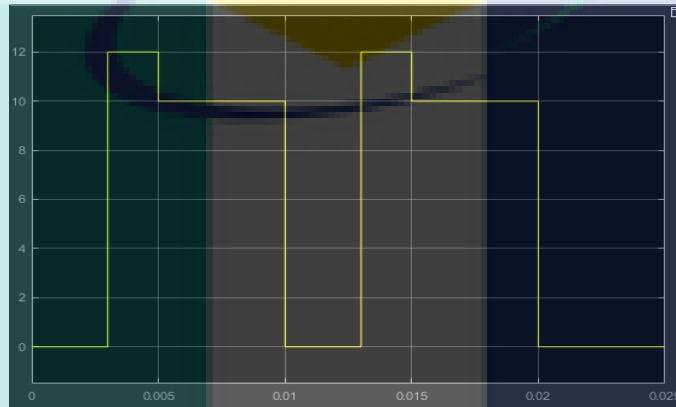
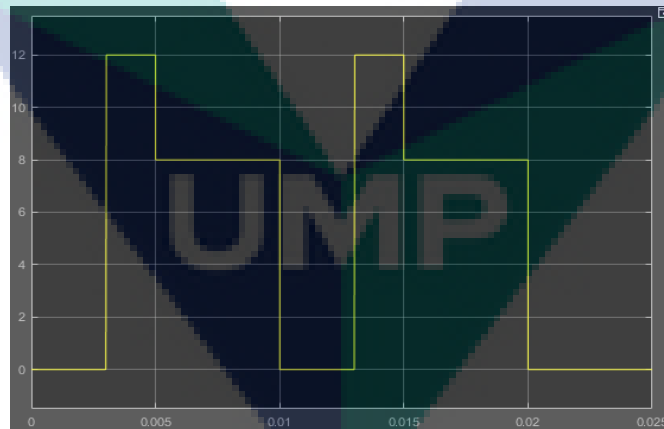


Figure 21 : Square wave signal

Figure 21 shows pulse signal (square wave) that mostly applied in an injector. This signal is control and set to be 12V at the peak and completed two cycles in 25ms. This signal is used as a comparison between other 6 signals to identify the best mass flow rate that can be used in an injector. Seven different input signals are identified from various sources to test on the injector model. Graph showing the voltage (v) against time (s) of input signal in Figure 22, Figure 23, Figure 24, Figure 25, Figure 26 and Figure 27 respectively.



**Figure 22 : Signal 1**



**Figure 23 : Signal 2**



The signal of this injector in Figure 22 has a peak 12V that quickly open the nozzle for 0.002s before it is drop to 10V. During 10V, the injector has a lower hold current rating that keep it open for duration of 0.005s. At 0.01s the signal is drop again to 0V and the peak current quickly opens the injector 0.003s after that. In Figure 23, the voltage is selected until 8V but the time remains the same.

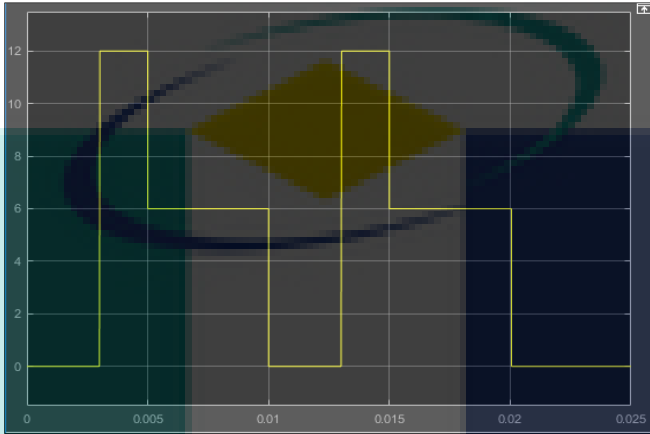


**Figure 24 : Signal 3**

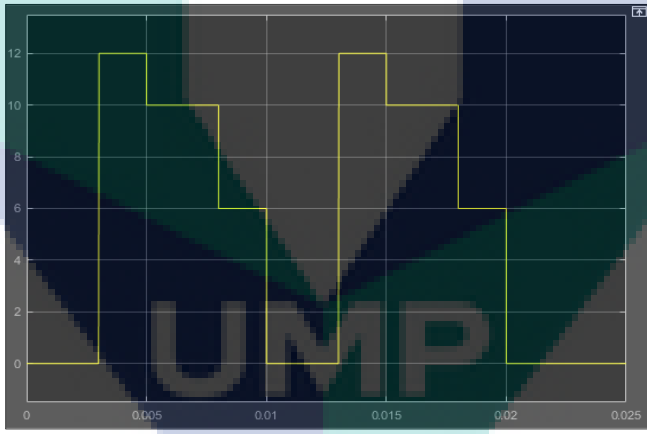


**Figure 25 : Signal 4**

Signal in Figure 24 also has a peak 12V since its using the same injector. The nozzle opens quickly for 0.002s then is drop to 6V. During 6V, the injector has a lower hold current rating that keep it open for duration of 0.005s. At 0.01s the signal is drop to 0V and the peak current quickly opens the injector 0.003s

after that. Figure 25 having a step signal where it set 2 times at 10V and 6V. During 10V, the injector holds for 0.003s and 6 volts it holds for 0.002s.

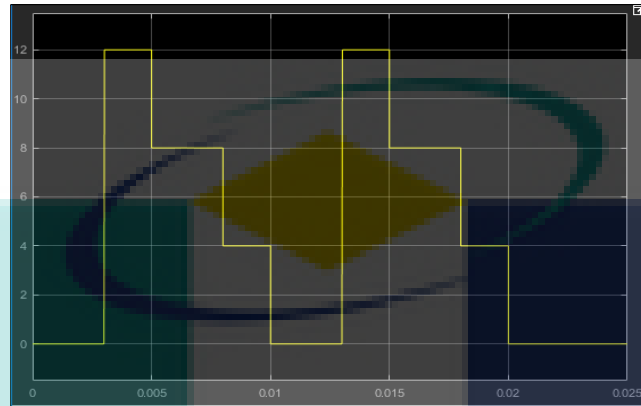


**Figure 26 : Signal 5**

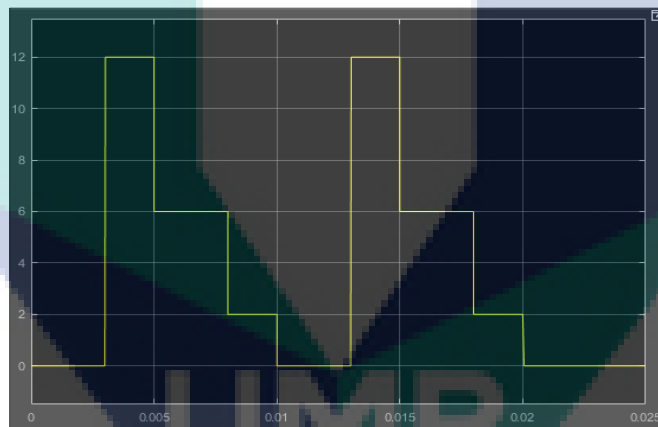


**Figure 27 : Signal 6**

Both signal in Figure 26 and Figure 27 has a peak of 12V. Signal 5 drop voltage at 8V and 4V. During 8V, it takes 0.003s hold before it drops to 4V. At 4V it takes 0.002s then it drops to 0V. Signal Figure 27 drop at 6V and 2V with the same time taken as Figure 26.

These entire signals are created by using builder signal in Matlab Simulink. The voltage drop and time injection can be control by entering the value into the builder signal. After all the characteristic are fulfil, the research proceeds to determine different input signal that can be test in the injector. Identify all the possible signal input that can be used in injector. All possible signals are tested on the first stage which is 10ms. From the model of injector in Simulink, the mass flow rate, mass, solenoid force and area nozzle of every input signal is taken.

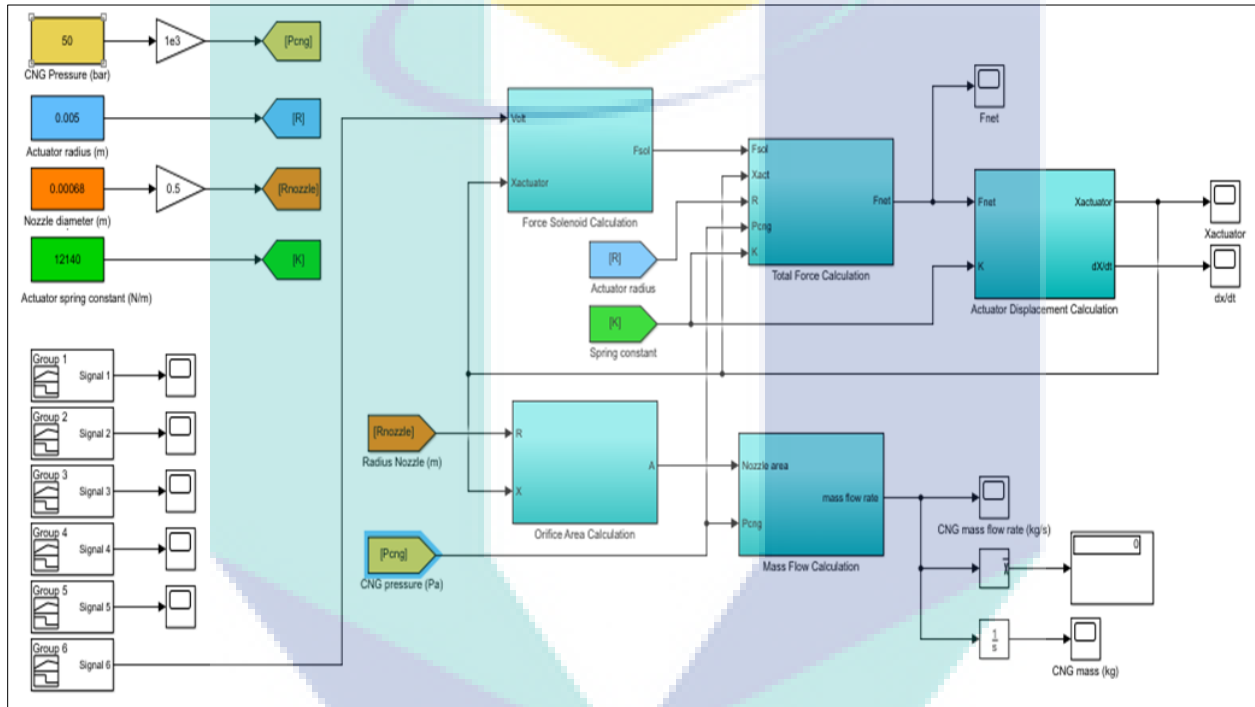


**Figure 28 : MATLAB Simulink block diagrams of the modified injector simulation model**

## RESULT & DISCUSSION

### 4.1 ANSYS Maxwell simulation result

#### 4.1.1 *Magnetic Field Intensity*

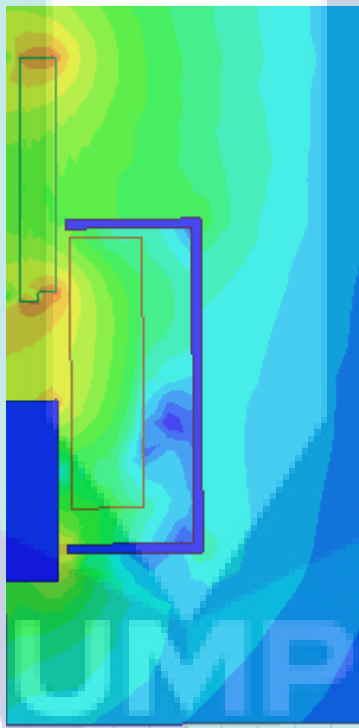


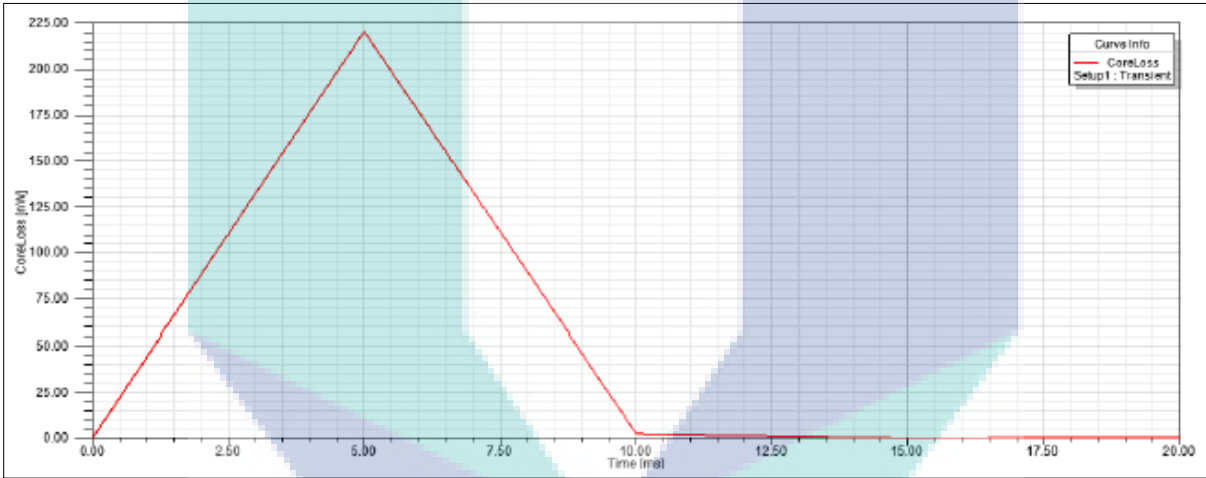
**Figure 29 : Magnetic Field Intensity simulation**

Magnetic fields are created by the movement of electrical particles and the intrinsic magnetic moments of particles associated with their spin's fundamental quantum property. Magnetic fields and electrical fields are interrelated and are both components of electromagnetic force one of the four fundamental forces of nature. In this study, it shows that magnetic field intensity is high at core of injector

because the core is magnetic material. The armature and yoke is non-magnetic material so there is no magnetic field intensity for both of the components. The material for coil is copper where it is use to generate current for the injector and the magnetic field produce hence it accumulate at the core because the core use the magnetic to attract the armature moving up and down when injector spray the fuel to combustion chamber.

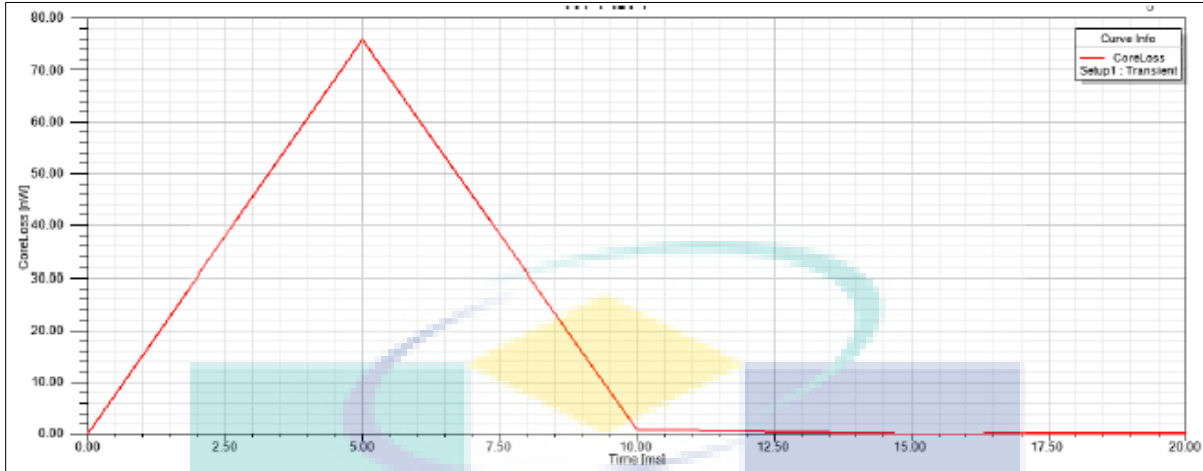
**4.1.2 Core Losses**

As stated above, a core loss is the loss that occurs in a magnetic core due to alternating magnetization which is the sum of the hysteresis loss and the eddy current loss. The figure below shown the core losses occur in range time of 20 ms.



**Figure 30 : Core losses at 6V**

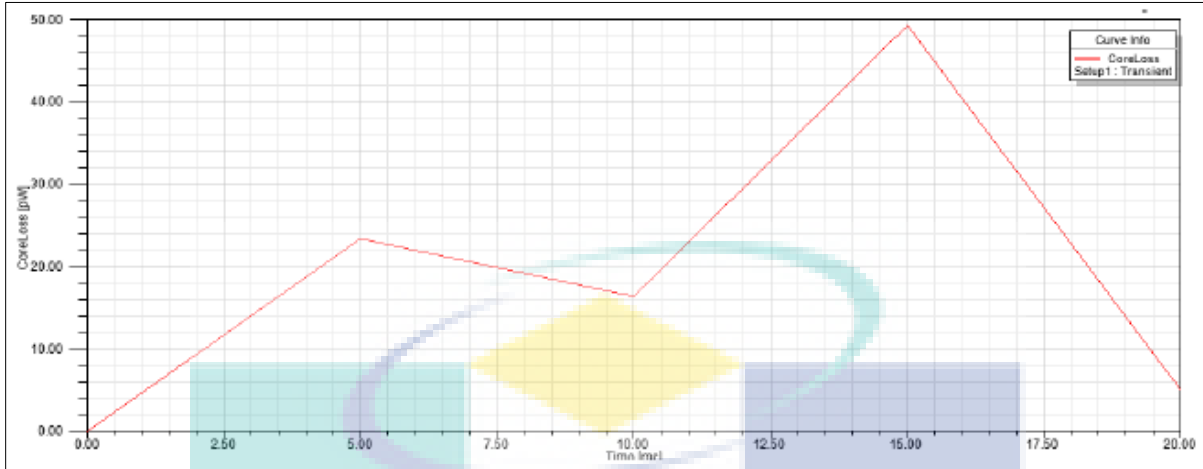
As shown in Figure 30; the voltage at 6V, resistance is 1.5 ohm and current is 8A. When the voltage is 6V, it reaches the highest core losses at 5ms which is about 225 nW. It take from 0ms to 5ms to reach the peak of core losses which voltage peak for the injector known as opening stage. After the 5ms, the losses start to decrease slowly to 0 since this is the closing stage for the injector. It takes about 10ms for entire injector process.



**Figure 31 : Core losses at 9V**

Figure 31 shows the losses when voltage at 9V. The current and resistance remain unchanged which is 8A and 1.5ohm. From 0ms to 5m the losses increase to the peak which 75 nW. At the 5ms, it reach the peak voltage of injector then from 5ms to 10 ms, the losses decrease to 0 which mean this is the end of the injector process. The pattern graph for 6V and 9V is similar but with different value of losses. The value of losses for the 6V is higher than 9V which mean it will affect the performance injector. The core loss is in a form of magnetic loss.

UMP



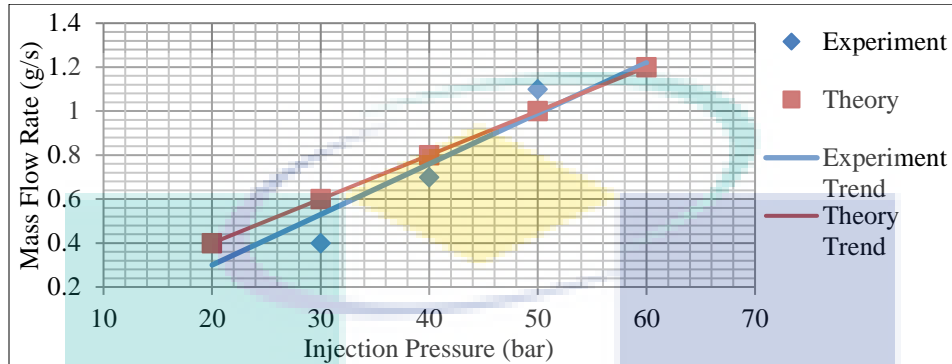
**Figure 32 : Core losses at 12V**

Figure 32 shows the simulation of injector electromagnetic behaviour when input voltage increases to the 12V. From 0ms to 5ms it shows an increasing in core losses around 20nW, then it decrease to 18nW at 10ms. After that, from 10ms to 15ms it increases again to 50nW which is the peak of losses in this 12V input. Compare to 6V and 9V, the time taken for 12V input to reach the peak losses is at 15ms while for 6V and 9V is 5ms. There is no any changing in current and resistance for every different input voltage.

UMP

## 4.2 Square wave experimental result

### 4.2.1 Case 1: effect of injection pressure



**Figure 33 : Comparison of injection pressure with mass flow rate**

Figure 33 show the effect of injection pressure with mass flow rate results summary. Based on the graph, the mass flow rate is linearly increased as the injection pressure increased. For injection pressure 30 bar, 40 bar, and 50 bar the increasing mass flow rate is in between 35 % to 40 %. The increment of the mass flow rate is not linear as expected by theoretical calculation as a result between 20 bar and 30 bar shows no increment. Between 50 bar and 60 bar, the increment is only 10 %. It is noticeable that the mass flow rate will increase linearly with increased injection pressure. The increased injection pressure has provided a larger mass delivery to the injector. It has enabled the a higher amount of mass flowing through the nozzle. As a summary, higher injection pressure will increase the mass flow rate.



#### 4.2.2 Case 2: effect of injection duration

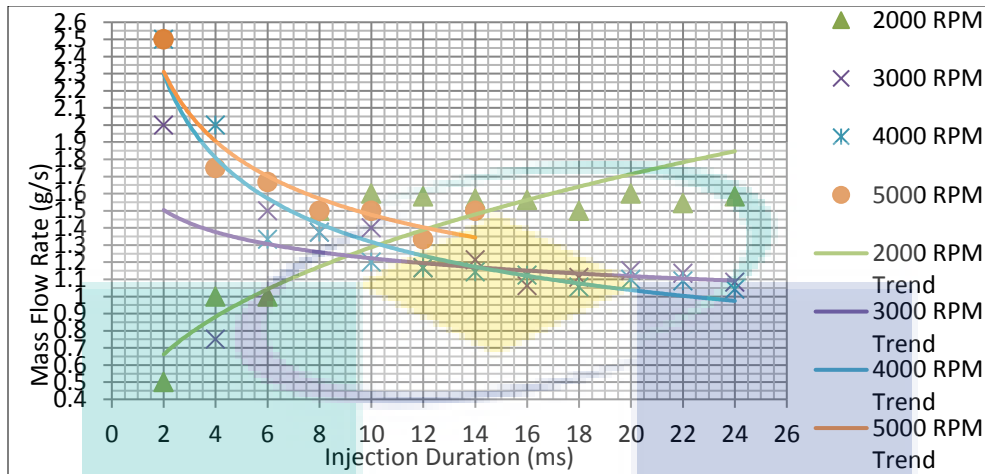


**Figure 34 : Comparison of mass flow rate on different injection duration**

Figure 34 presents a comparison of the mass flow rate graph based on different injection duration at different engine speed (RPM). The mass flow rate patterns show a higher fluctuation at low injection duration lower than 10 ms at all engine speed. After 10 ms, the mass flow rate plot gradually becomes constant. However, at the engine speed of 2000 RPM the mass flow rates showing an increasing trend. The maximum mass flow rate recorded was 2.5 g/s at 5000 RPM and the minimum mass flow rate recorded was 0.5 g/s at 2000 RPM. Theoretically, the mass flow rate is constant at a specific engine speed or frequency. The real reasons for this fluctuation especially at short injection duration are due to the inconsistent effective opening time of the injector nozzle.

### 4.2.3 Case 3: Effect of Injection Frequency

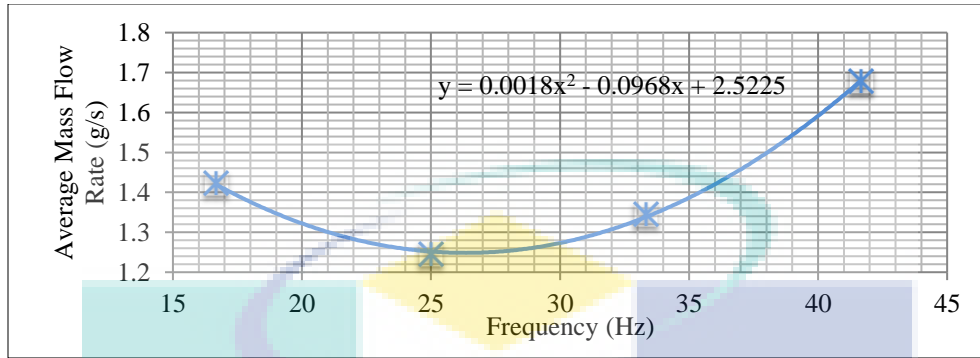


**Figure 35 : The measured average mass flow rate at different injection frequency**

Figure 35 presents the measured average mass flow rate at different injection frequency. The measured average mass flow rate shows a polynomial trend where the minimum average mass flow rate is obtain at the injection frequency of 25 Hz. Theoretically, the average mass flow rate will increase linearly with increased of injection frequency since the injection duration is fixed. The reason of this nonlinearity is due to highly fluctuated data at low injection frequency of 2000 RPM and 3000 PRM.

UMP

### 4.3 Two stage signal wave experimental result

#### 4.3.1 Square wave and two stage signal wave profile

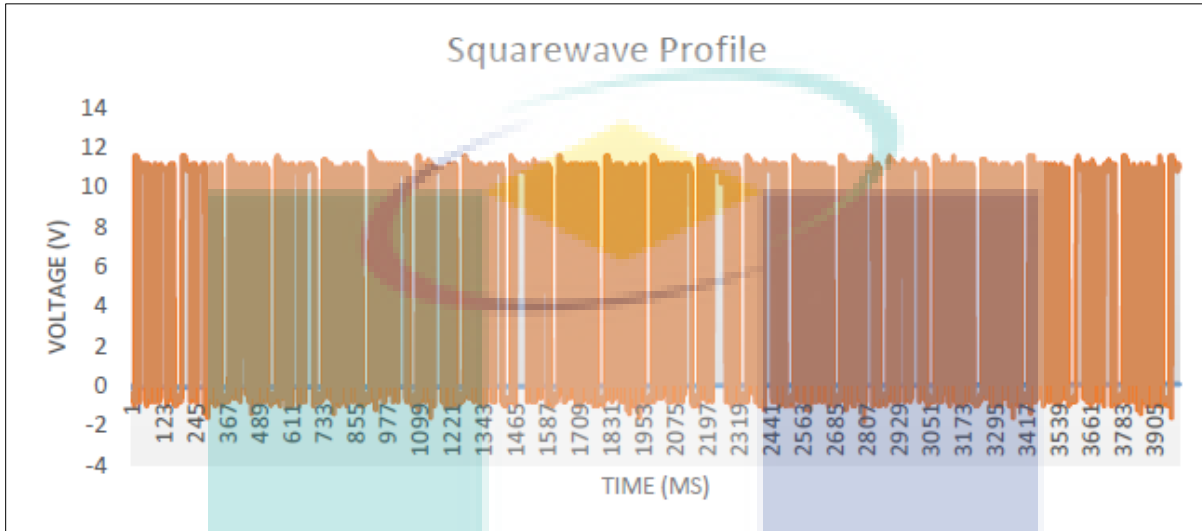


Figure 36 : Square wave profile at 50bar

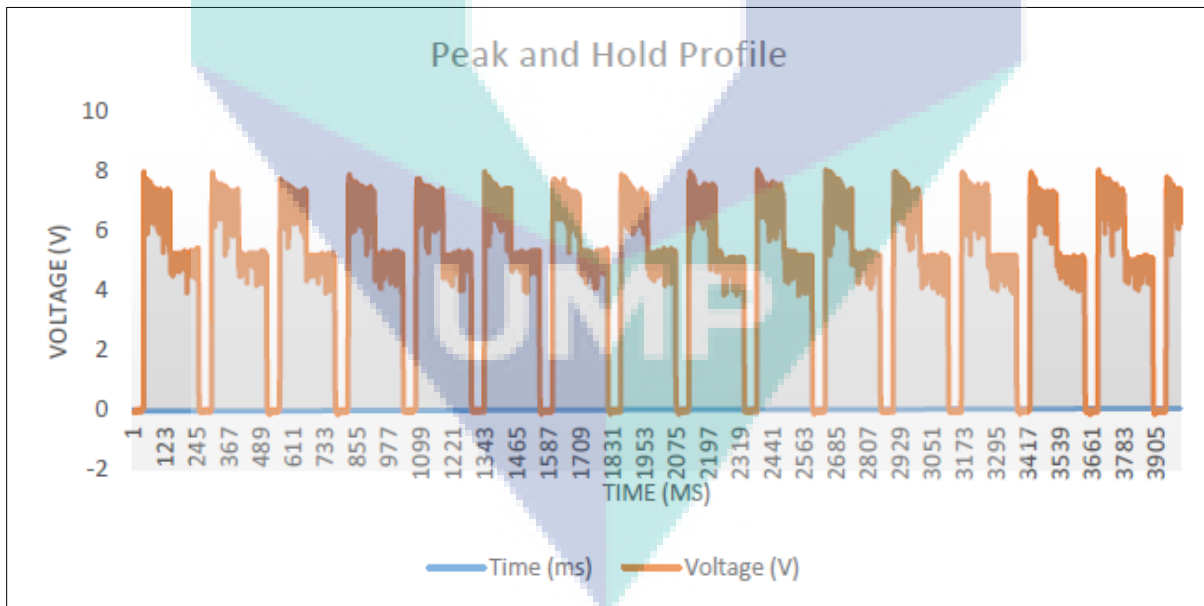


Figure 37 : Two stage signal wave profile at 50bar

Figure 36 and Figure 37 shows the different shape of waveform produce at 50 bar pressure with different control strategy. The duration for one cycle each waveform is same at 5ms per cycle with direct power supply of 12V. Square wave profile was created using standard motor driver with duration for on time 4ms and duration of off time 1ms each cycle. When connected to the load, the voltage reading was drop to 11V. For peak and hold profile, when connected to load the voltage was drop at 8V for peak and 5.5V for hold time. The duration time that was set to is peak 2ms, hold 2ms, and 1ms for closing time.

#### 4.3.2 Case 1: fixed duration time

For Case 1, the duration for one cycle is fixed to 5ms for both square wave and peak and hold profile at 50 bar pressure. On time and closing time for square wave profile was 4ms and 1ms respectively. While peak, hold and closing time for peak and hold profile was 2ms, 2ms and 1ms respectively. This experiment was conducted until 40ms injection duration. The mass flow rate for both signals can be calculated through the gradient of each trendline from the graph.

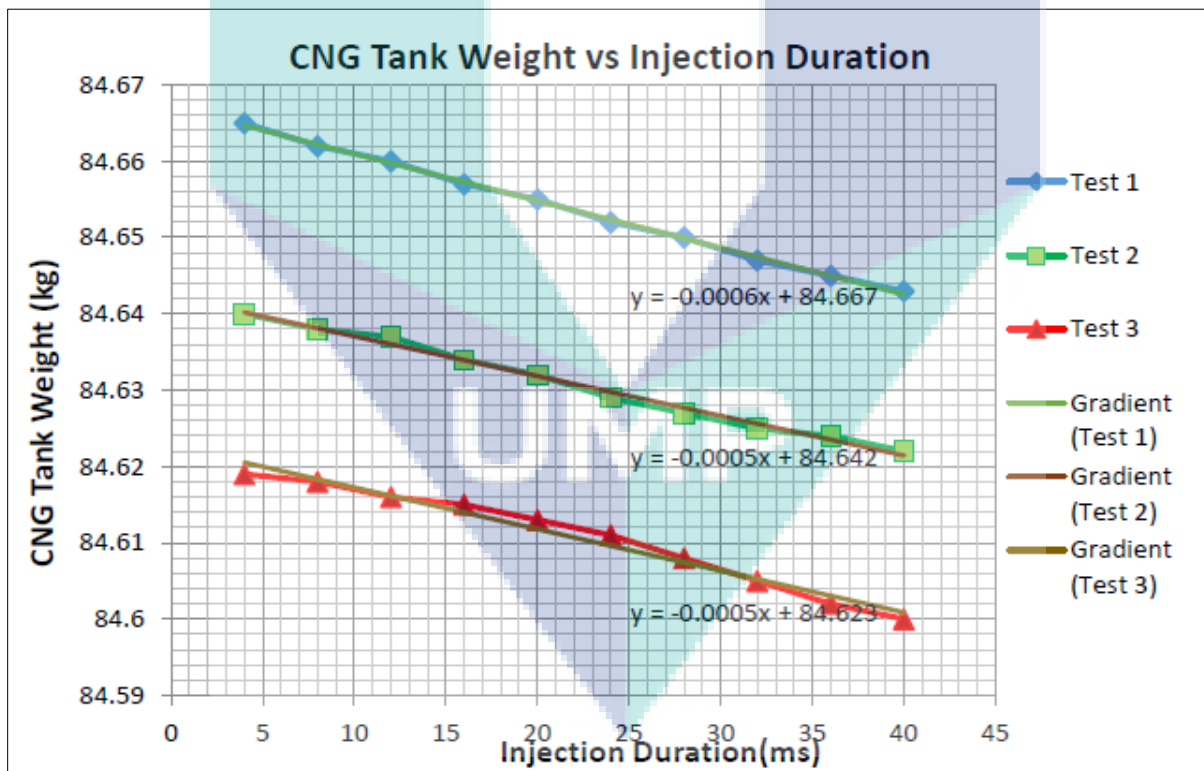
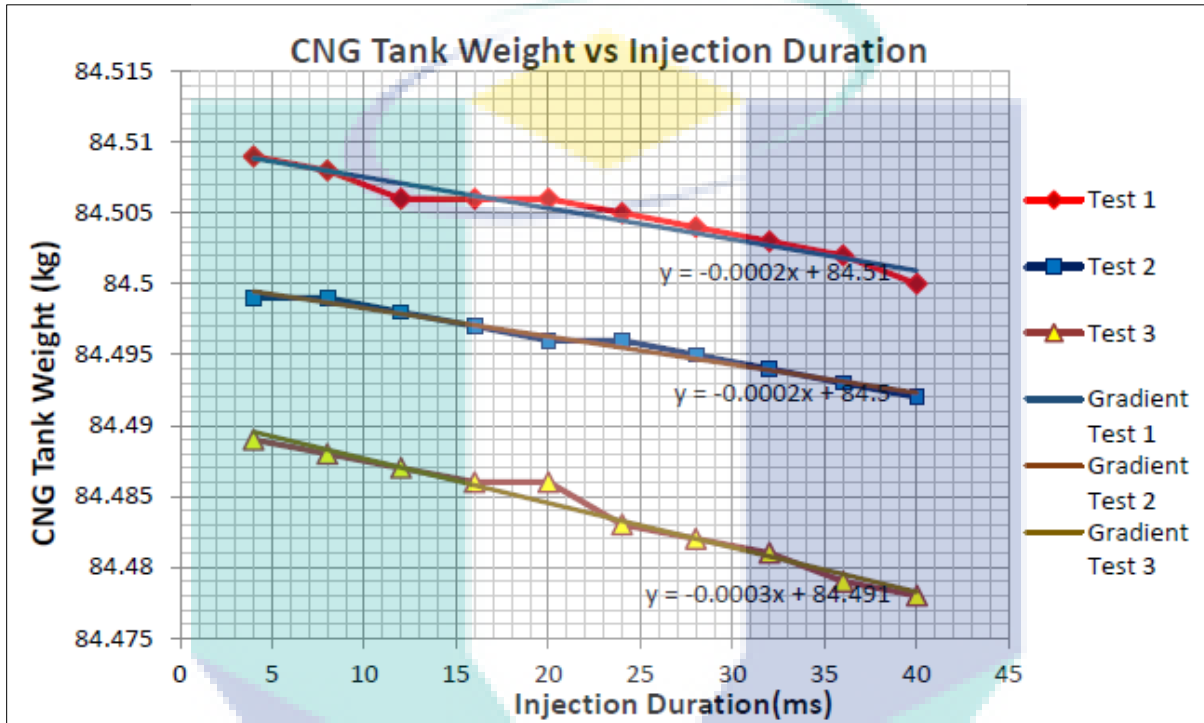


Figure 38 : CNG tank weight vs injection duration for square wave

From the result of Figure 38, it is shown that the trendline for CNG tank weight was linearly decreasing proportional to the injection duration. The testing was repeated three times and the mass flow rate can be calculated through the gradient of each trendline. From the graph above, we can see that the mass flow rate for square wave is between 0.5 g/s and 0.6 g/s.



**Figure 39 : CNG tank weight vs injection duration for two stage signal wave**

From the graph of Figure 39, it is shown that the trendline for CNG tank weight was linearly decreasing proportional to the injection duration. This testing was also repeated three times and the mass flow rate had been collected. From the graph above, we can see that the mass flow rate for peak and hold signal is between 0.2 g/s and 0.3 g/s.

#### 4.3.3 Case 2: increasing duration time

For Case 2, duration for one cycle waveform is change for both square wave and peak and hold profile. It started at 4ms to 24ms with interval of 3ms. For square wave, the close time was fix to 1ms and open time

was varied. For peak and hold profile, peak duration time fix at 2ms and close time fix at 1ms respectively while hold duration time was varied. This experiment is executed at constant CNG pressure of 50 bars and 1000 injection counts. The mass flow rate then is calculate through the change of mass of CNG tank divide by injection duration time.

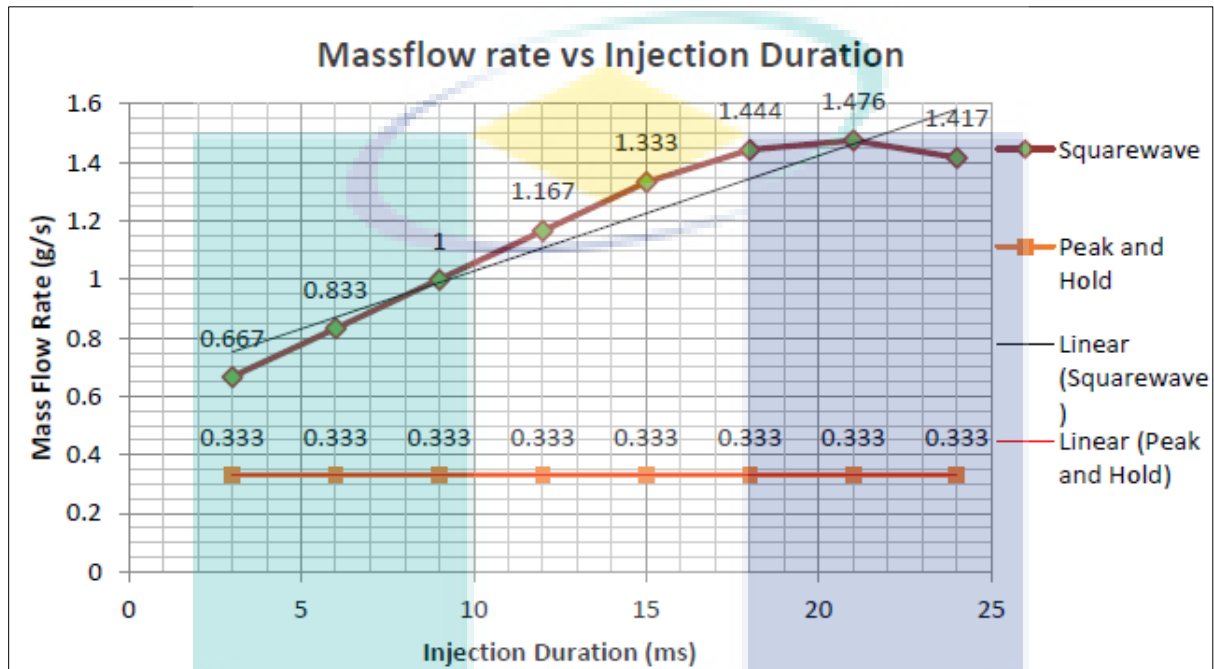


**Figure 40 : Mass flow rate of square wave and two stage signal wave**

From the comparison in Figure 40, it is shown that control strategy for peak and hold signal gave a lowest mass flow rate than square wave profile. Increasing injection duration give a different effect to a both signal. The graph shown that mass flow rate for square wave is linearly increase from 0.6 g/s until 1.4 g/s while for peak and hold profile is steadily constant at 0.3g/s.

In Case 1, the measured mass flow rate is higher for square wave signal than peak and hold signal. However, both had the same trend where CNG tank weight is linearly decreased as the injection duration increase for all three tests. For Case 2, with variable time duration, the mass flow rate was higher than in Case 1. With control of injection time we can reduce and increase injection time with result in change of mass flow rate. Mass flow rate for square wave signal is linearly increased due to increasing opening time

injection. However, for peak and hold signal it shows no changing in mass flow rate. This is because, at hold phase, injector is not in open state rather it is at closing position which cause no changing to the mass flow rate.

#### 4.4 Square wave simulation result

##### 4.4.1 Validation of Simulation Model (Injection Pressure)

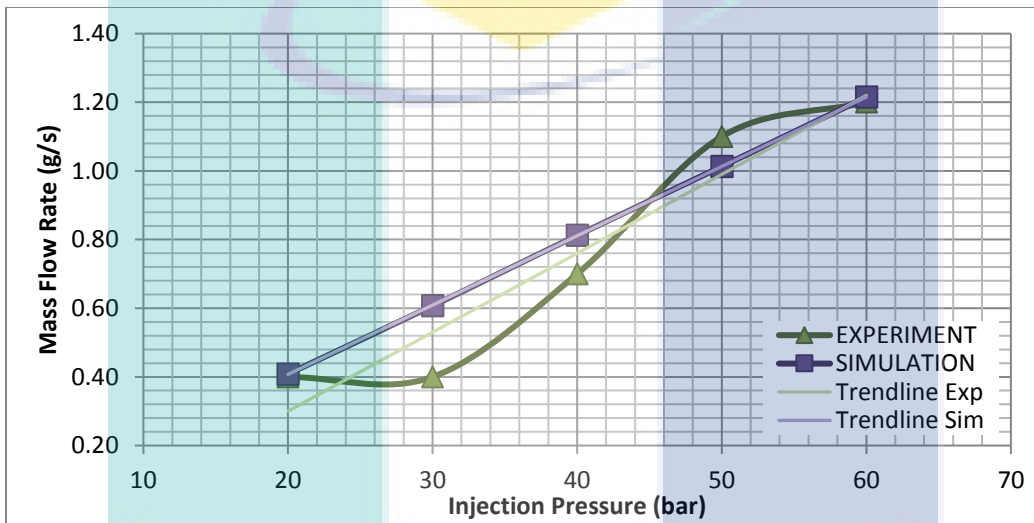


**Figure 41 : Comparison between experiment and simulation injection pressure**

Figure 41 shows the tabulation data between experiment and simulation result. The mass flow rate was measured at the injection pressure of 20 bar, 30 bar, 40 bar, 50bar and 60 bar for both experiment and simulation result. Based on the graph, both experiment and simulation result shows a linearly increasing trendline. It is proven that simulation result follow the experimental result trend. Thus, the simulated result therefore is valid for reference. There are just a small differences margin between the simulation and experiment result. The highest different mass flow rate between experiment and simulation is at 30bar at 52%. As a summary, simulation model can predict the expected result.

#### 4.4.2 Validation of Simulation Model (Injection Duration)

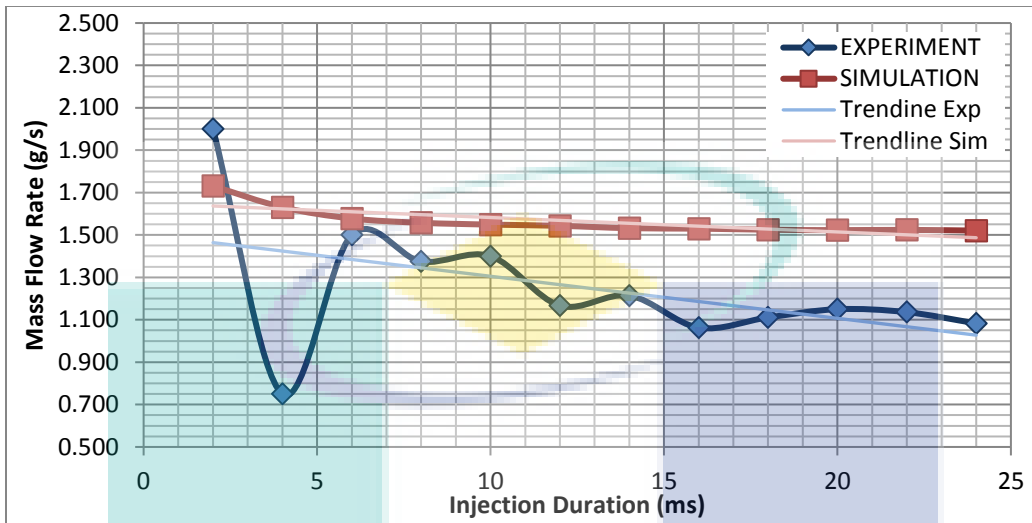


**Figure 42 : Comparison between experiment and simulation injection duration**

Figure 42 shows the tabulation data between experiment and simulation result. The mass flow rate for experiment and simulation result was measured at the injection duration of 2 ms to 24 ms with the increment of 2 ms for each injection duration increments. Based on the graph, both experiment and simulation result shows a linearly decreasing trendline. . Thus, it is proven that simulation result follow the experimental result trend. There are moderate differences margin between the simulation and experiment result. Although the simulated results have a moderate differences margin between experiment result, it is still valid for reference. The highest different mass flow rate between experiment and simulation is at 4ms at 117%. As a summary, simulation model can only predict the trend at moderate accuracy.



#### 4.4.3 Parametric Study of Input Voltage

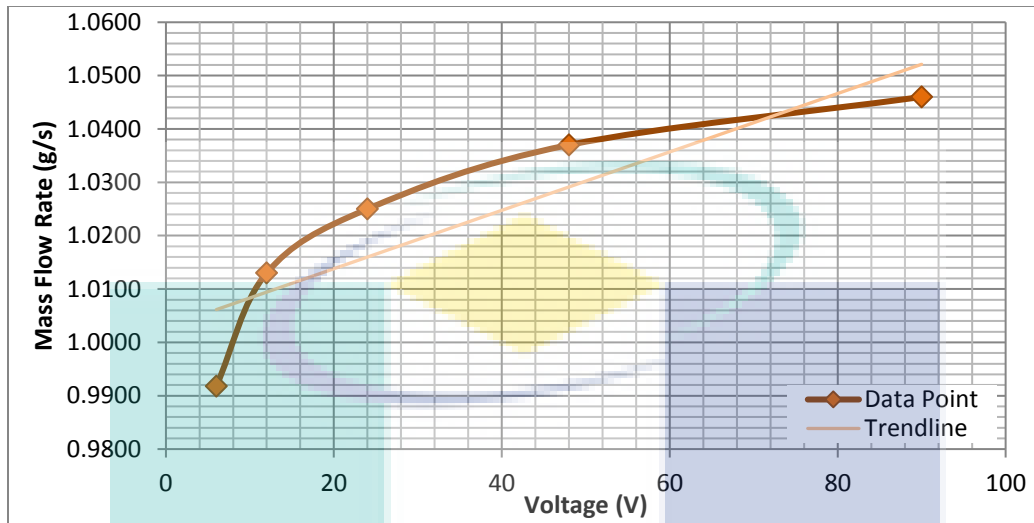


**Figure 43 : Simulation result of input voltage versus mass flow rate**

Figure 43 shows the simulation result of input voltage versus mass flow rate. The mass flow rate for simulation result was measured at the voltage value of 6 V, 12 V, 24 V, 48 V and 90 V. Based on the graph, the simulated data show a linearly increasing trendline. Therefore, an increasing in the input voltage will directly affect the mass flow rate of the injector. The higher the input voltage is, the longer time it takes for the signal to turn off the armature. Thus, there will be more gas flow through the injector nozzle. As a summary, if the input voltage increases, then mass flow rate will also increase.

#### 4.4.4 Parametric Study of Spring Constant

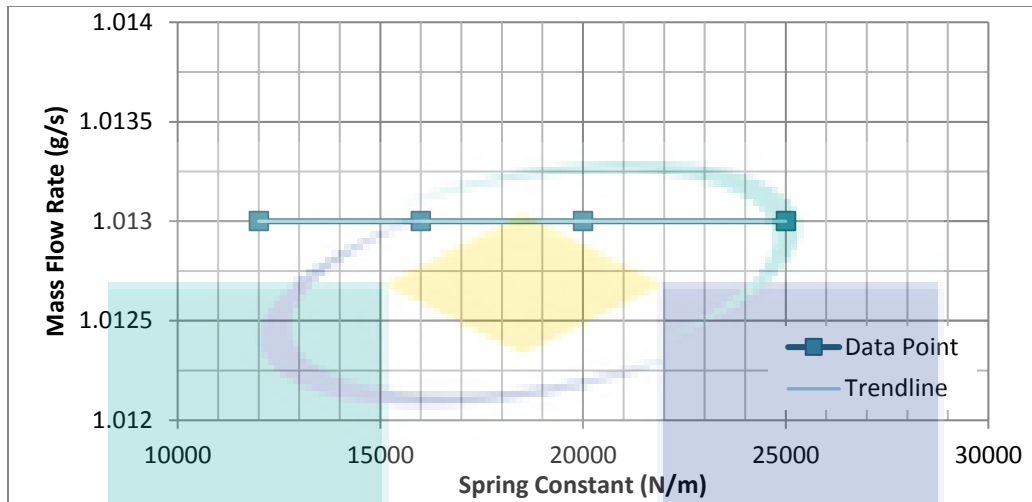


**Figure 44 : Simulation result of spring constant versus mass flow rate**

Figure 44 shows the simulation result of spring constant versus mass flow rate. The mass flow rate for simulation result was measured at the spring constant value of 12000 N/m, 16000 N/m, 20000 N/m and 25000 N/m. Based on the graph, the simulated data show a linear trendline. Therefore, an increasing in spring constant value will not affect the mass flow rate of the injector. Spring stiffness only affect the opening and closing time of armature but not needle lift height. To add up, spring stiffness also affects a tiniest bit of the opening and closing time of armature making it insignificant. Thus, the mass flow rate for the injector will remain the same. As a summary, if spring constant increases, then mass flow rate will remain the same value.

#### 4.4.5 Parametric Study of Nozzle Diameter

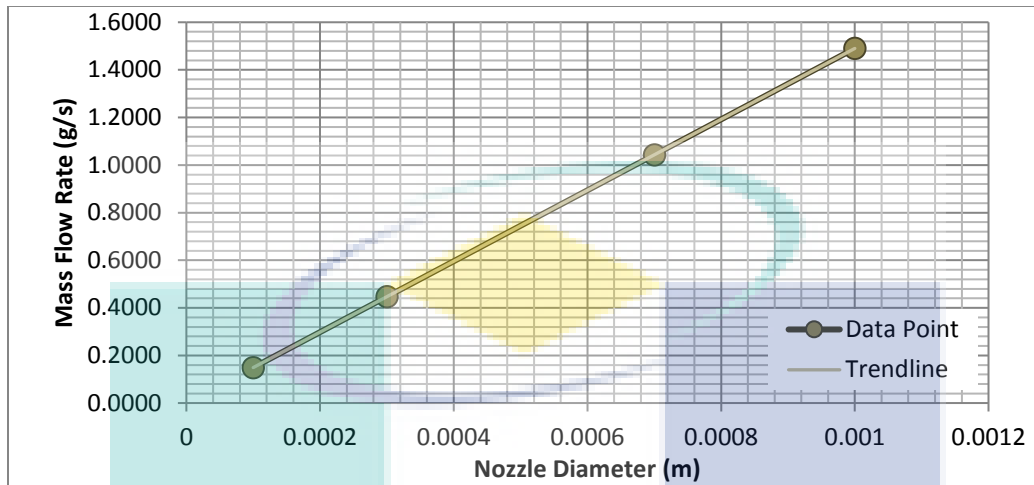


**Figure 45 : Simulation result of nozzle diameter versus mass flow rate**

Figure 45 shows the simulation result of nozzle diameter versus mass flow rate. The mass flow rate for simulation result was measured at the nozzle diameter size of 0.0001 m, 0.0003 m, 0.0007 m and 0.0010 m. Based on the graph, the simulated data show a linearly increasing trendline. Therefore, an increasing in nozzle diameter size will directly affect the mass flow rate of the injector. A larger nozzle diameter size gives more space for gas to flow through the nozzle hence increases the mass flow rate of the injector. As a summary, if the nozzle diameter size increases, then mass flow rate will also increase.

#### 4.4.6 Parameter Study of Armature Mass

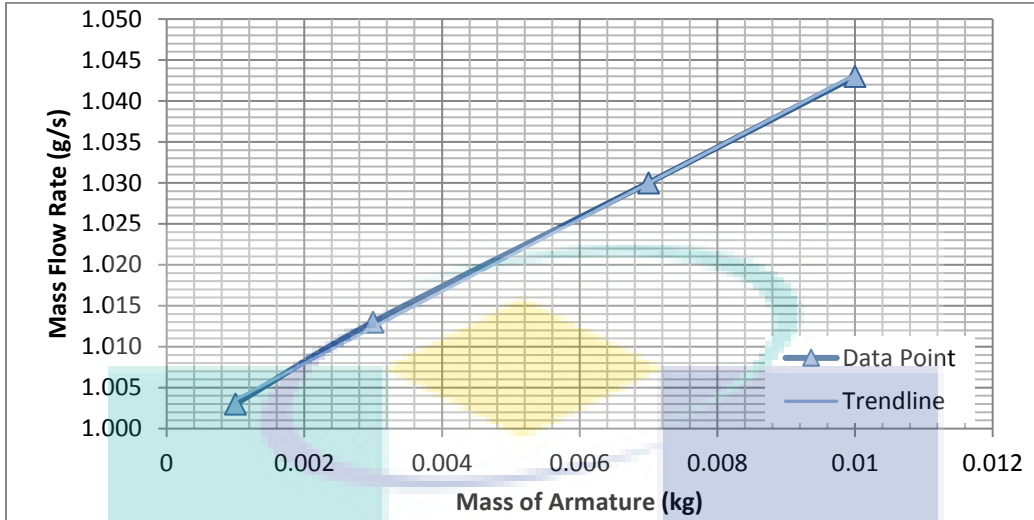


**Figure 46 : Simulation result of armature mass versus mass flow rate**

Figure 46 shows the simulation result of armature mass versus mass flow rate. The mass flow rate for simulation result was measured at the nozzle diameter size of 0.001 kg, 0.003 kg, 0.007 kg and 0.010 kg. Based on the graph, the simulated data show a linearly increasing trendline. Therefore, an increasing in armature mass will directly affect the mass flow rate of the injector. The heavier armature mass is, the longer time it takes for the spring to overcome the force. Thus, it provides a longer time for the gas to flow through the injector nozzle. As a summary, if armature mass increases, then mass flow rate will also increase.

#### 4.4.7 Parametric Sensitivity Ranking

**Table 7 : Parametric sensitivity ranking**

Ranking	Parametric Factor	Sensitivity Value	Unit
1	Nozzle Diameter (m)	1489.705	(g/s/m)
2	Armature Mass (kg)	337.667	(g/s/kg)

3	Injection Duration (s)	40.520	(g/s/s)
4	Input Voltage (V)	0.0844	(g/s/V)
5	Injection Pressure (bar)	0.0203	(g/s/bar)
6	Spring Constant (N/m)	0.0000834	(g/s/N/m)

Table 7 shows the sensitivity result of each parameter thus its ranking of sensitivity. Nozzle Diameter has the highest sensitivity with the value of 1489.705 g/s/m while Spring Constant has the lowest sensitivity with the value of 0.0000834 g/s/N/m. As a summary, each of parameter sensitivity have been identified and ranked accordingly.

#### 4.5 Two stage signal wave simulation result

##### 4.5.1 Nozzle area

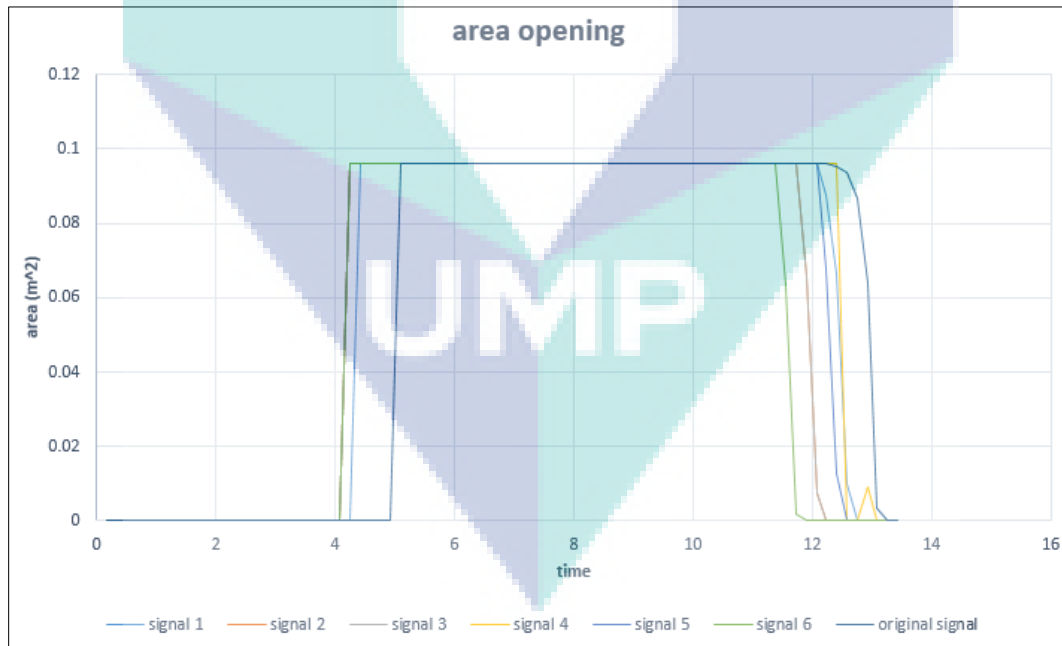


**Figure 47 : Nozzle area simulation result**

The maximum nozzle area opening for the injector model is  $0.096\text{m}^2$ . The entire signal reached the maximum area opening including the original signal. The orifice effect on the injector fuel nozzle area indicated power, indicated torque and performance of direct-injection engine. Area nozzle opening will affect the mass flow rate since the amount of fuel jet into the chamber is based on the area orifice.

#### 4.5.2 Solenoid force

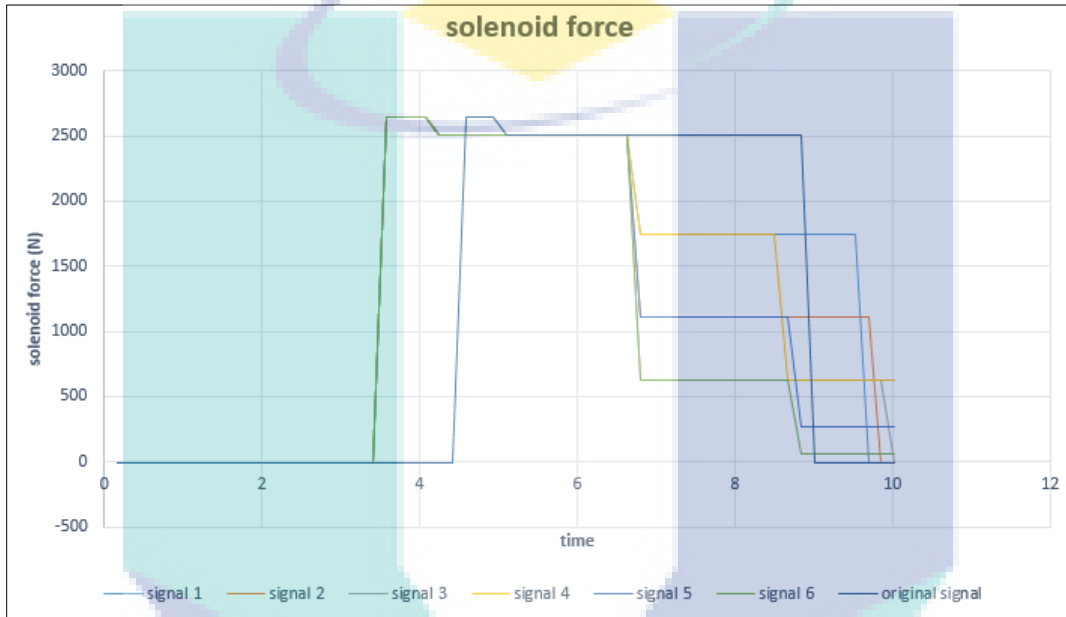


**Figure 48 : Solenoid force simulation result**

The maximum solenoid force recorded is 2510N. Original signal shows a late peak compared to the other 6 signals. This graph shows that solenoid need more force during opening (peak) of the injector before it is hold. During hold process, solenoid only took 2500N which is 10N difference from the peak. Solenoid force will affect the opening of nozzle area.

### 4.5.3 Total mass inject

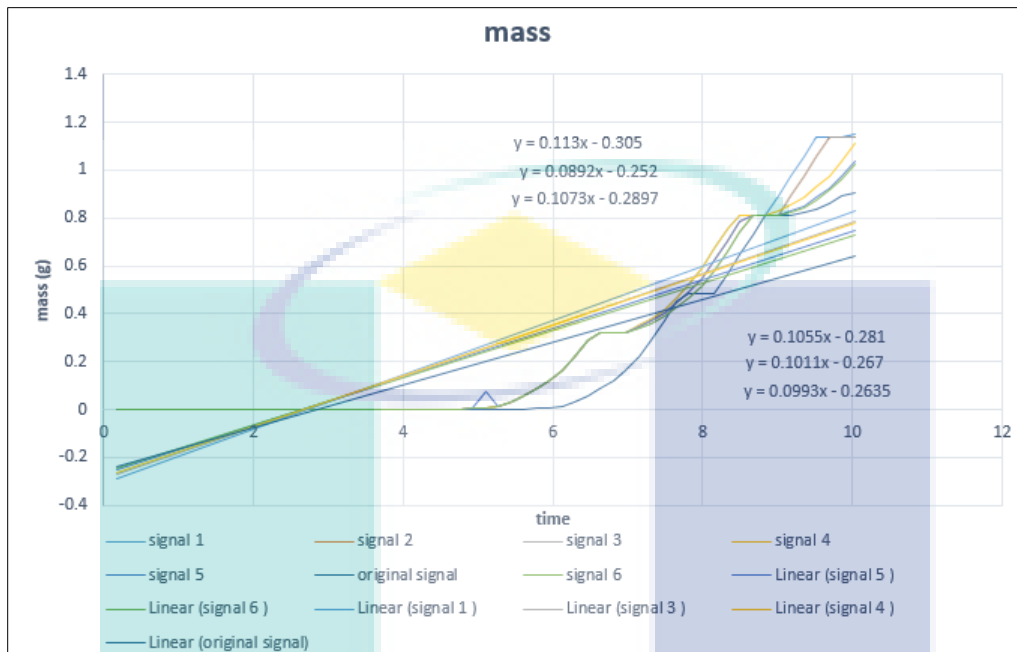


**Figure 49 : Total mass inject simulation result**

The highest total mass injected in 10ms is signal 1 which is 1.147g. Since the result for area opening and solenoid force are same, so it's complicated to determine which signal is better. From mass vs time graph it shows that the highest amount is signal 1 and the lowest is square wave. The highest mass injected also influenced the mass flow rate in the injector. The gradient of this graph represent of the mass flow rate.

UMP

#### 4.5.4 Mass flow rate

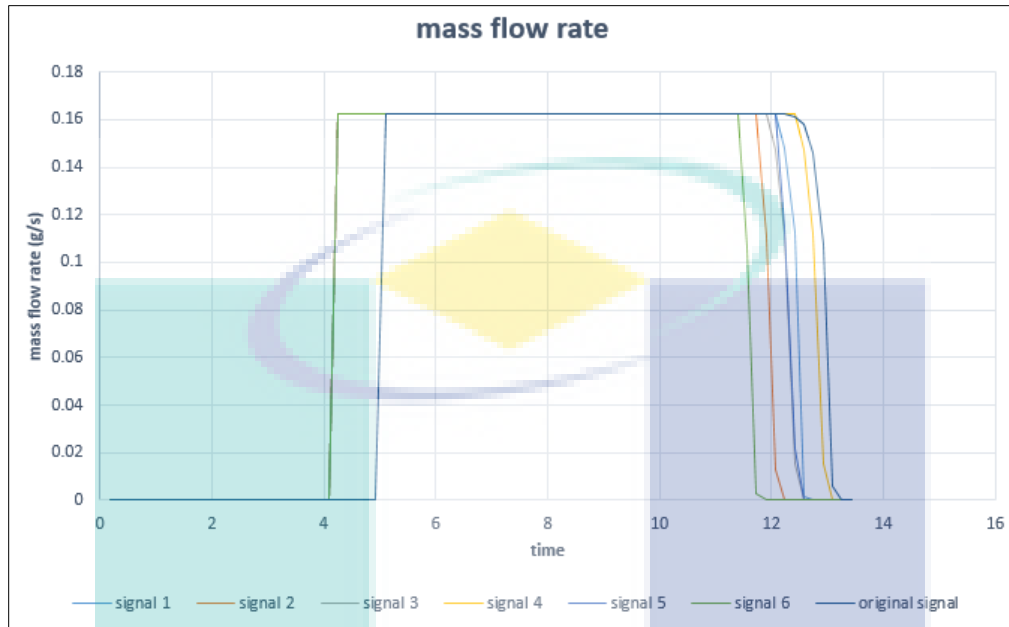


**Figure 50 : Mass flow rate simulation result**

The maximum mass flow rate is 0.162 g/s. All signal reached the maximum mass flow rate.

#### 4.5.5 Result comparison

**Table 8 : Mass flow rate simulation comparison**

Input Signal	Mass flow rate (g/s)	Percentage Difference (%)
Signal 1	0.113 (g/s)	26.97 %
Signal 2	0.109 (g/s)	22.47 %
Signal 3	0.107 (g/s)	20.22 %
Signal 4	0.106 (g/s)	19.10 %
Signal 5	0.101 (g/s)	13.48 %
Signal 6	0.099 (g/s)	11.24 %
Original Signal	0.089 (g/s)	-



**Table 9 : Mass flow rate simulation and experiment comparison**

Input Signal	Maximum Mass Flow Rate Simulation (g/s)	Average Mass Flow Rate Simulation (g/s)	Mass Flow Rate Experiment (g/s)
Square Wave	0.16 (g/s)	0.08 (g/s)	0.6 (g/s)
Two Stage	0.14 (g/s)	0.07 (g/s)	0.2 (g/s)

From Table 8 shows the mass flow rate in simulation for signal 1 shows the highest percentage difference which is 26.97%. Signal 1 also recorded 0.113g/s which are the highest mass flow rate compare to other signal. Table 9 shows the mass flow rate in experiment for two different signals. Square wave shows 0.16g/s while two stage signal shows 0.14 g/s value of mass flow rate. The difference mass flow rate simulation and experiment for square wave is 0.44 g/s and for two stage is 0.06 g/s.



## CONCLUSION

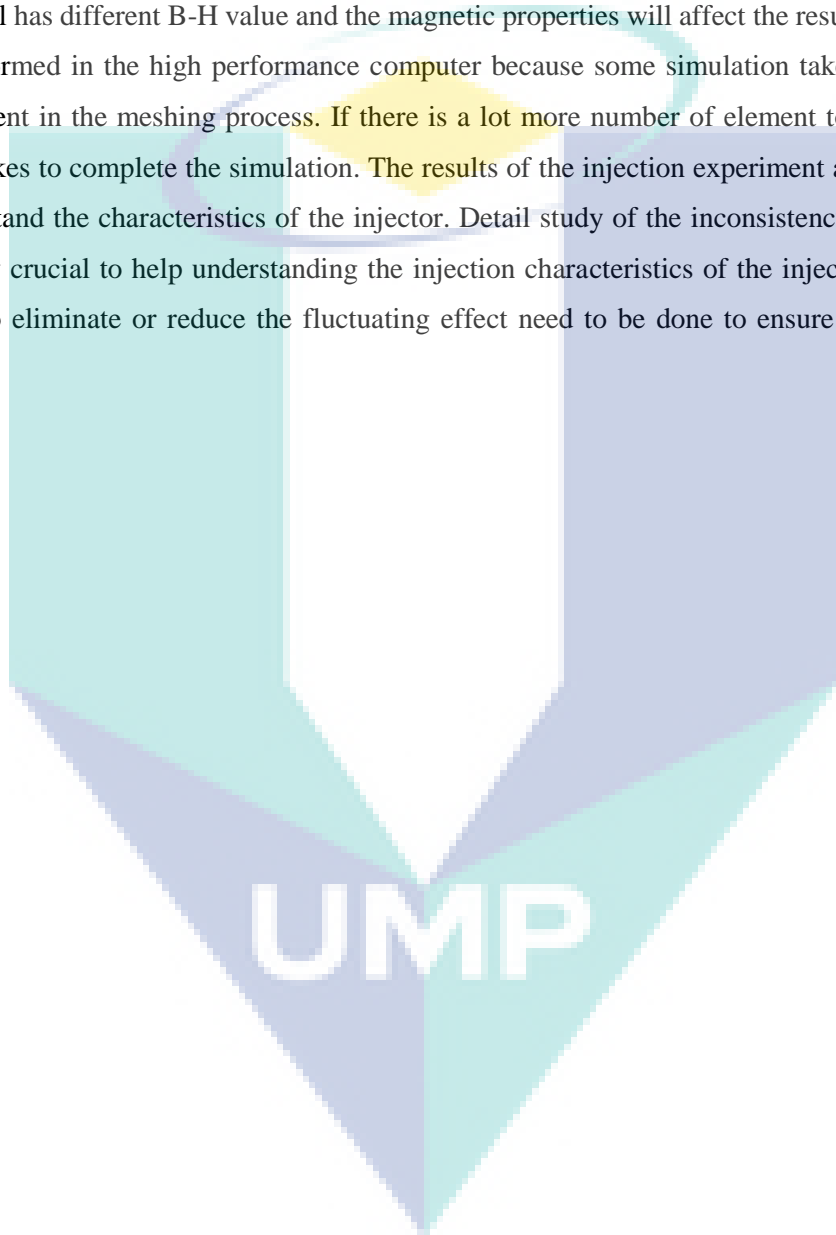
Unable to run using Ansys Workbench, it is found that ANSYS Maxwell is able to made this electromagnetic simulation after some research and study from previous paper. Next is choosing the simulation to run either in 2D or 3D. For 3D, when import to the ANSYS it is unable to run since there always have geometry error. For 2D, the design must be fulfil the experiment need which is the position of core, coil and other component in right place. The result of losses were acquired the simulation but cannot be validate with the experiment result since there no experimental data for this injector model hence the result is consider as rough estimation only.

Experimental work has been carried out to describe the injection characteristics of CNG fuel on a single-hole direct injector. Injection pressure linearly affected the mass flow rate of injector. The degree of mass flow rate fluctuation is higher at short injection duration compared to long injection duration. The fluctuation also affected the mass flow rate at lower frequency. The theoretical calculations of the injector were unable to predict the fluctuating trend. Based on the control strategy of standard motor driver that produce square wave signal, it shown that it will consume a lot more of fuel consumption than control strategy of peak and hold signal. This was proved by the different of mass flow rate between both strategies. Fuel injector for static and dynamic properties is important because it will affect the mixture formation and combustion in combustion chamber of vehicle. Based on the result, it is concluded that due to short period cyclic operation and short injection duration, the opening and closing of injector are not perfectly done.

A simulation model was built to recreate the experimental work that has been carried out to study the injection characteristics of CNG fuel on a single-hole direct injector. The simulation model can predict the mass flow rate of direct injector trendline but cannot detect the fluctuation in short injection duration. Some of the parameter will affect the mass flow rate of direct injector and some will have no effect on the mass flow rate. The most significant parameter affected the mass flow rate sensitivity was Nozzle Diameter followed by Armature Mass, Injection Duration, Input Voltage, Injection Pressure and Spring Constant. The mass flow rate really influences by the shape of the signal. The result shows a high increasing of

percentage when using a two-step signal. Two step input signal give more momentum for the open and closed injector in order to give a good value of mass flow rate. The simulation model of the injector able to predict the mass flow rate trend but were unable to spot the fluctuating trend.

In depth study is needed about the injector material for the component inside the injector. The different material has different B-H value and the magnetic properties will affect the result. The simulation need to be performed in the high performance computer because some simulation take time depend the number of element in the meshing process. If there is a lot more number of element to be compute, the longer time it takes to complete the simulation. The results of the injection experiment and simulation are useful to understand the characteristics of the injector. Detail study of the inconsistency of injector mass flow rate is very crucial to help understanding the injection characteristics of the injector better. Further study on how to eliminate or reduce the fluctuating effect need to be done to ensure injector optimum performance.



## REFERENCES

1. Kalam, M.A. and H.H. Masjuki, An experimental investigation of high performance natural gas engine with direct injection. *Energy*, 2011. 36(5): p. 3563-3571.
2. Erfan, I., et al., Injection characteristics of gaseous jet injected by a single-hole nozzle direct injector. *Fuel*, 2015. 160: p. 24-34.
3. Cheng, Q., Z. Zhang, and N. Xie, Power losses analysis of the gasoline direct injector within different driven strategies. *Applied Thermal Engineering*, 2016. 91(April): p. 611-621.
4. Huang, D., et al., Design of Drive Circuit for GDI Injector. *IEEE*, 2011: p. 6-9.
5. Zhang, X., et al., Direct Fuel Injector Power Drive System Optimization. *SAE Int. J. Engines*, 2014. 7(3).
6. Visconti, P., et al., Driving electronic board with adjustable piloting signal parameters for characterization of Common Rail diesel injectors with pure Biodiesel. *IEEE*, 2016.
7. Lino, P., G. Maione, and F. Saponaro, Fractional-Order Modeling of High-Pressure Fluid-Dynamic Flows: An Automotive Application. *IFAC-PapersOnLine*, 2015. 48(1): p. 382-387.
8. Lino, P., et al. Parameter estimation in non-linear models of pressure dynamics in CNG injection systems. in *2015 IEEE International Conference on Industrial Technology (ICIT)*. 2015.
9. Mohd, M., Ali, M. S., Salim, M. A., Bakar, R. A., Fudhail, A. M., Hassan, M. Z., & S, A. M. M. (2015). Performance analysis of a spark ignition engine using compressed natural gas ( CNG ) as fuel. *Energy Procedia*, 68, 355–362.  
<https://doi.org/10.1016/j.egypro.2015.03.266>
10. Pourkhesalian, A.M., A.H. Shamekhi, and F. Salimi, Alternative fuel and gasoline in an SI engine: A comparative study of performance and emissions characteristics. *Fuel*, 2010. 89(5): p. 1056-1063.

11. Cho, H.M. and B.Q. He, Spark ignition natural gas engines-A review. *Energy Conversion and Management*, 2007. 48(2): p. 608-618.
12. Sen, A.K., J. Zheng, and Z. Huang, Dynamics of cycle-to-cycle variations in a natural gas direct-injection spark-ignition engine. *Applied Energy*, 2011. 88(7): p. 2324-2334.
13. Sementa, P., B. Maria Vaglieco, and F. Catapano, Thermodynamic and optical characterizations of a high performance GDI engine operating in homogeneous and stratified charge mixture conditions fueled with gasoline and bio-ethanol. 2012. 96(Complete): p. 204-219.
14. Song, J., Choi, M., & Park, S. (2017). Comparisons of the volumetric efficiency and combustion characteristics between CNG-DI and CNG-PFI engines. *Applied Thermal Engineering*, 121, 595–603.  
<https://doi.org/10.1016/j.applthermaleng.2017.04.110>
15. Baratta, M., & Rapetto, N. (2014). Fluid-dynamic and numerical aspects in the simulation of direct CNG injection in spark-ignition engines. *Computers & Fluids*, 103, 215–233.  
<https://doi.org/10.1016/j.compfluid.2014.07.028>
16. Baratta, M., & Rapetto, N. (2015). Mixture formation analysis in a direct-injection NG SI engine under different injection timings. *Fuel*, 159, 675–688.  
<https://doi.org/10.1016/j.fuel.2015.07.027>
17. Choi, M., Song, J., & Park, S. (2016). Modeling of the fuel injection and combustion process in a CNG direct injection engine. *Fuel*, 179, 168–178.  
<https://doi.org/10.1016/j.fuel.2016.03.099>
18. Moon, S. (2018). Potential of direct-injection for the improvement of homogeneous-charge combustion in spark-ignition natural gas engines. *Applied Thermal Engineering*, 136, 41–48. <https://doi.org/10.1016/j.applthermaleng.2018.01.068>
19. Chitsaz, I., et al., Experimental and numerical investigation on the jet characteristics of spark ignition direct injection gaseous injector. 2013. 105: p. 8-16.
20. Hajialimohammadi, A., et al., Ultra high speed investigation of gaseous jet injected by a single-hole injector and proposing of an analytical method for pressure loss prediction during transient injection. *Fuel*, 2016. 184: p. 100-109.

21. Garrappa, R., et al., Model Optimization and Flow Rate Prediction in Electro-injectors of Diesel Injection Systems. *IFAC PapersOnLine*, 2016. 49(11): p. 484-489.
22. Wang, H.P., D. Zheng, and Y. Tian, High pressure common rail injection system modeling and control. *ISA Transactions*, 2016. 63: p. 265-273.
23. Lino, P., B. Maione, and C. Amorese, Modelling and predictive control of a new injection system for compressed natural gas engines. *Control Engineering Practice*, 2008. 16(10): p. 1216-1230.
24. Lino, P. and G. Maione, Design and Simulation of Fractional-Order Controllers of Injection in CNG Engines. *IFAC Proceedings Volumes*, 2013. 46(21): p. 582-587.
25. Lino, P. and G. Maione, Switching Fractional-Order Controllers of Common Rail Pressure in Compressed Natural Gas Engines. *IFAC Proceedings Volumes*, 2014. 47(3): p. 2915-2920.
26. Hideyuki Watanabe, Shinya Ichise, Takahiro Nagaoka, Development of compact and high performance fuel injector using electromagnetic field simulation[C], SAE paper 2005-32-0019, 2005.
27. F. Bircher, P. Marmet, Multiphysics modeling of a micro valve, in: *Proceedings of the European COMSOL Conference*, Milan, Italy, 2009. Paper No. 6679.
28. Motoyuki Abe, Noriyuki Maekawa, Yoshihito Yasukawa, et al., Quick response fuel injector for direct-injection gasoline engines[J], *J. Eng. Gas Turb. Power* 134 (2012) 1e5.
29. S.V. Angadi, R.L. Jackson, Song-Yul Choe, et al., Reliability and life study of hydraulic solenoid valve. Part 1: a multi-physics finite element model [J], *Eng. Fail. Anal.* 16 (2009) 874e887.
30. Dean Cvetkovic, Irena Cosic, Aleksandar Subic, Improved performance of the electromagnetic fuel injector solenoid actuator using a modelling approach [J], *Int. J. Appl. Electromagn. Mech.* 27 (2008) 251-273.
31. Klaus Mutschler, Shivam Dwivedi, Sabrina Kartmann, et al., Multi physics network simulation of a solenoid dispensing valve[J], *Mechatronics* 24 (2014) 209-221.

32. Mohan, B., Yang, W., Yu, W., Tay, K. L., & Chou, S. K. (2015). Numerical investigation on the effects of injection rate shaping on combustion and emission characteristics of biodiesel fueled CI engine. *Applied Energy*, 160, 737–745. <https://doi.org/10.1016/j.apenergy.2015.08.034>
33. Stegemann J, Seebode J, Baltes J, Baumgarten C, Merker GP. Influence of throttle effects at the needle seat on the spray characteristics of a multihole injection nozzle. *Zaragoza 2002*;9:11.
34. Seebode J, Merker GP, Lettmann H. Injection strategies under the influence of pressure modulation and free rate shaping in modern di-diesel engines. *CIMAC Congr 2004*.

